4.4. Coupons

In this section, photographs and microscopic evaluations of the approximately 12-in.-square metal coupon samples are presented. In Section 4.4.1, pre- and post-test photographs of each coupon type are shown. In Section 4.4.2, SEM/EDS results are presented, and the types of corrosion products found on the post-test coupons are discussed. In Section 4.4.3, evidence and discussion concerning the lack of corrosion on the aluminum coupons in Test #4 is given.

4.4.1. Pre- and Post-Test Coupon Photographs

Submerged Coupons

Figures 4-99 through 4-101 are pictures of submerged aluminum coupons from each test. Figure 4-102 shows an unused aluminum coupon. With the exception of Test #4, the test solution had a large effect on the aluminum coupons. Coupons in Tests #1 and #5 developed a brown coating on the surface, whereas coupons in Tests #2 and #3 accumulated white particle deposits across their surface. In addition, a copper layer was evident on the Tests #2 and #3 coupons. The layer can be attributed to electrochemical ion transfer. Tests #1 and #5 coupons had a more uniform distribution of deposit across their surface, whereas coupons in Tests #2 and #3 had more of a "blotchy" arrangement on their surfaces. The Test #4 coupon was relatively unchanged.

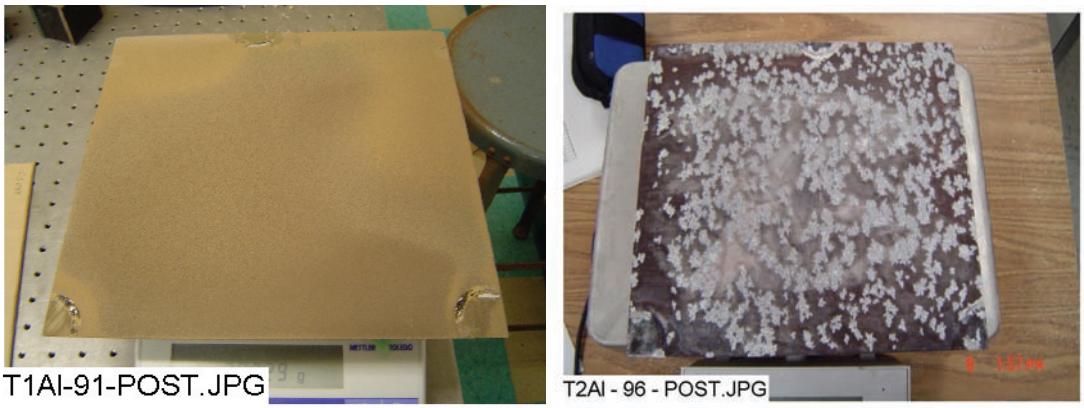

Figure 4-99. ICET Test#1 Al-91 post-test (left); ICET Test#2 Al-96 post-test (right).

Figure 4-100. ICET Test#3 Al-155 submerged, post-test (left); ICET Test#4 Al-237 submerged, post-test, (right).

Figure 4-101. ICET Test #5 Al-93 submerged, post-test.

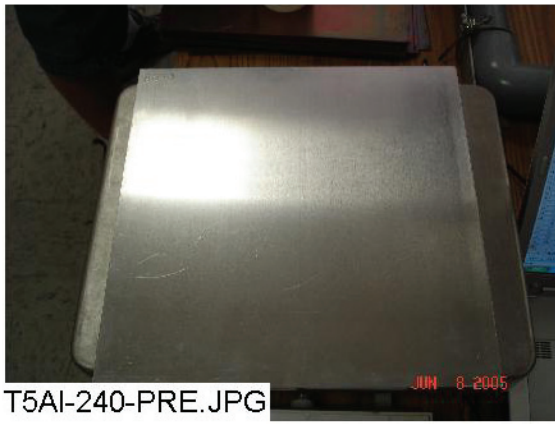

Figure 4-102. Unused Al coupon.

Figures 4-103 to 4-105 are pictures of submerged galvanized steel coupons from each test. Figure 4-106 shows an unused galvanized steel coupon. The galvanized steel coupons from Tests #1 and #5 appeared to have the same type of white deposit, although the deposition patterns are different. The deposits on these coupons were attached securely to the surface, although there was not a great amount of deposit. The Tests #2 and #3 coupons both accumulated a large amount of white particles on their surfaces. These particles could be rubbed off the coupon with relative ease. The Test #4 coupon appeared relatively unchanged from its pretest appearance.

Figure 4-103. ICET Test #1 GS-328 submerged, post-test (left); ICET Test #2 GS-335 submerged, post-test (right).

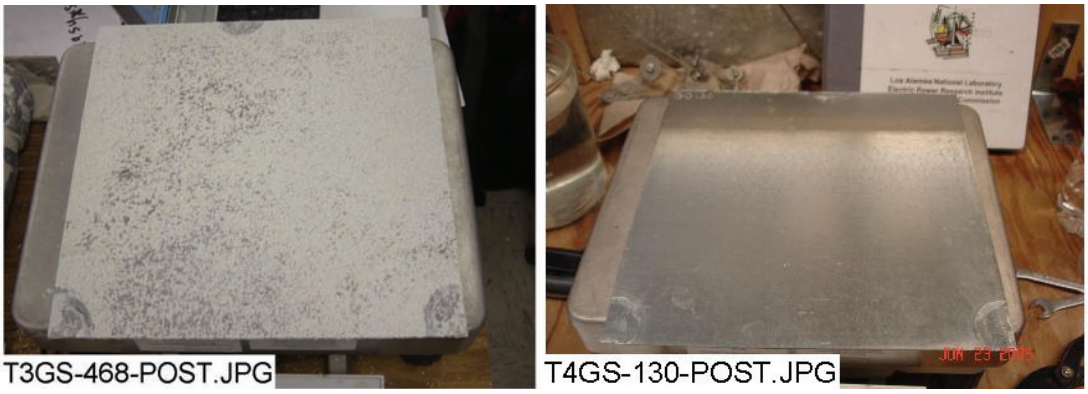

Figure 4-104. ICET Test #3 GS-468 submerged, post-test (left); ICET Test #4 GS-130 submerged, post-test (right).

Figure 4-105. ICET Test #5 GS-332 submerged, post-test.

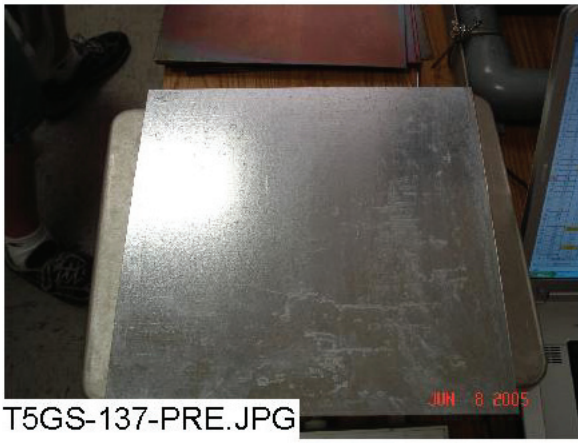

Figure 4-106. Unused GS coupon.

Figures 4-107 through 4-109 are pictures of submerged IOZ-coated steel coupons from each test. Figure 4-110 shows an unused IOZ-coated steel coupon. The Tests #1 and #5 coupons developed a brownish hue, with the color of Test #1 being more pronounced. The Test #2 coupon shows a relatively large amount of white deposit originating in the areas where the coupon came in contact with the rack. The Test #3 coupon had a small amount of white deposit in the areas where the coupon was in contact with the rack, as well as a small amount of white precipitate distributed across the surface of the coupon. The Test #4 coupon developed a small amount of white precipitate on the top edge of the coupon; however, it was not significantly changed from its pretest appearance.

Figure 4-107. ICET Test #1 IOZ-77 submerged, post-test (left); ICET Test #2 IOZ-79 submerged, post-test (right).

Figure 4-108. ICET Test #3 IOZ-156 submerged, post-test (left); ICET Test #4 IOZ-233 submerged, post-test (right).

Figure 4-109. ICET Test #5 IOZ-310 submerged, post-test.

Figure 4-110. Unused IOZ-coated coupon.

Figures 4-111 through 4-113 are pictures of submerged copper coupons from each test. Figure 4-114 shows an unused copper coupon. The coupons from Tests #1, #2, #4, and #5 have similar types of particle deposition. They all accumulated small amounts of white particles that were arranged in horizontal streaks across the coupon surface. The Test #3 copper coupon accumulated a large amount of white particles distributed across the coupon's entire surface. This deposition could be rubbed off relatively easily.

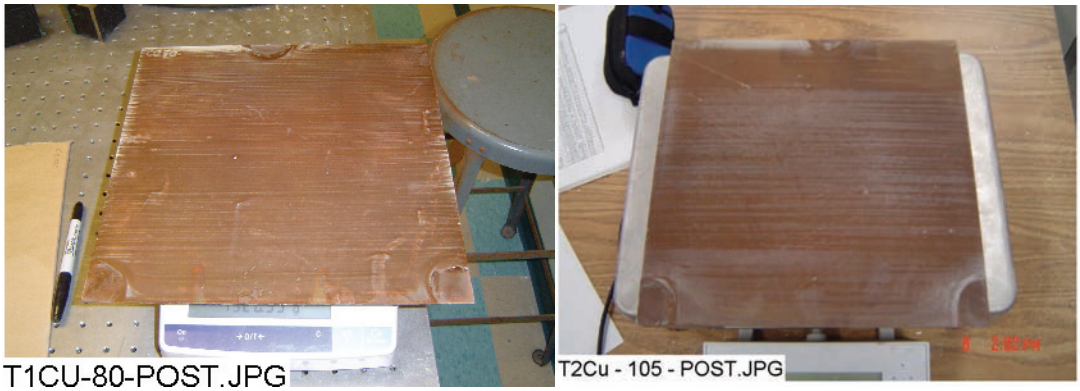

Figure 4-111. ICET Test #1 CU-80 submerged, post-test (left); ICET Test #2 CU-105 submerged, post-test (right).

Figure 4-112. ICET Test #3 CU-207 submerged, post-test (left); ICET Test #4 CU-100 submerged, post-test (right).

Figure 4-113. ICET Test #5 CU-100 submerged, post-test.

Figure 4-114. Unused CU coupon.

Figures 4-115 through 4-117 are pictures of submerged carbon steel (uncoated steel, US) coupons from each test. Figure 4-118 shows an unused carbon steel coupon. Tests #1 and #5 carbon steel coupons both accumulated a small amount of white particles on their surfaces. This

accumulation caused the surfaces to develop a dull, sandy finish. The Test #2 coupon developed a large amount of yellowish corrosion product on its surface, and its surface was roughened. The Test #3 coupon accumulated some white particles, distributed evenly over the surface of the coupon. Some yellowish corrosion also developed on the bottom edge of the coupon. The Test #4 coupon was largely unchanged from its pre-test condition.

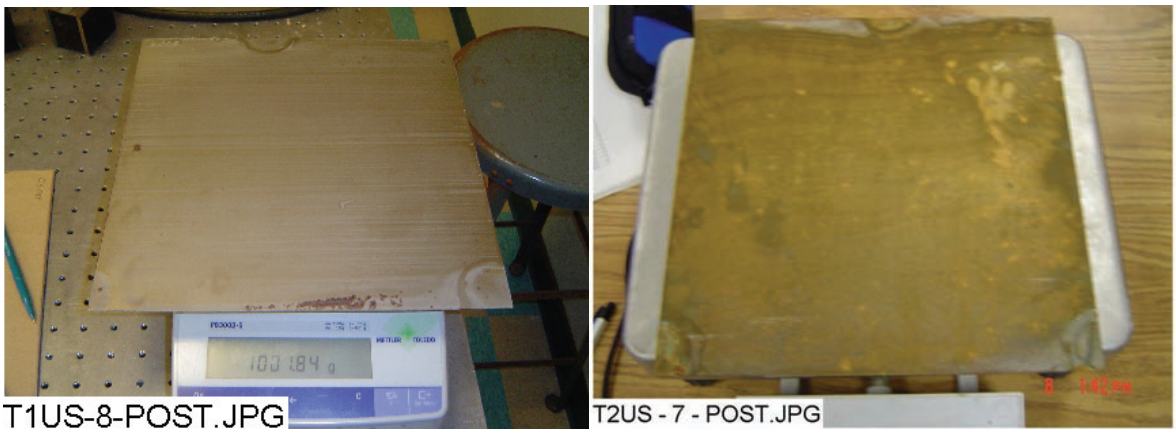

Figure 4-115. ICET Test #1US-8 submerged, pre-test (left); ICET Test #2 US-7 submerged, post-test (right).

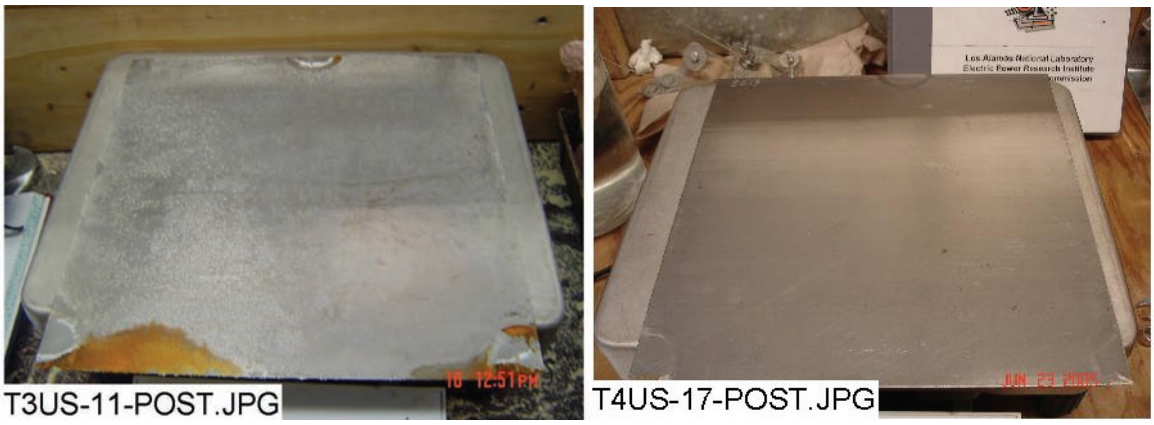

Figure 4-116. ICET Test #3 US-11 submerged, post-test (left); ICET Test #4 US-17 submerged, post-test (right).

Figure 4-117. ICET Test #5 US-14 submerged, post-test.

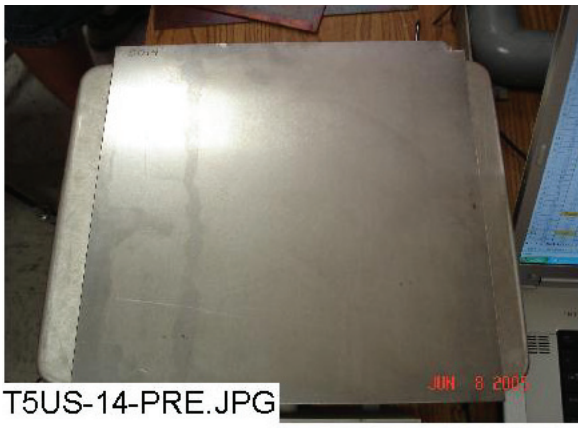

Figure 4-118. Unused US coupon.

Figures 4-119 through 4-121 are pictures of submerged concrete coupons from each test. Figure 4-122 shows an unused concrete coupon. Concrete coupons from Tests #1, #4, and #5 all developed a brownish color, with the coupons from Tests #1 and #5 having a deeper color change. The Test #2 coupon was relatively unchanged. The Test #3 coupon accumulated a large amount of white particles that were distributed evenly over the surface of the coupon.

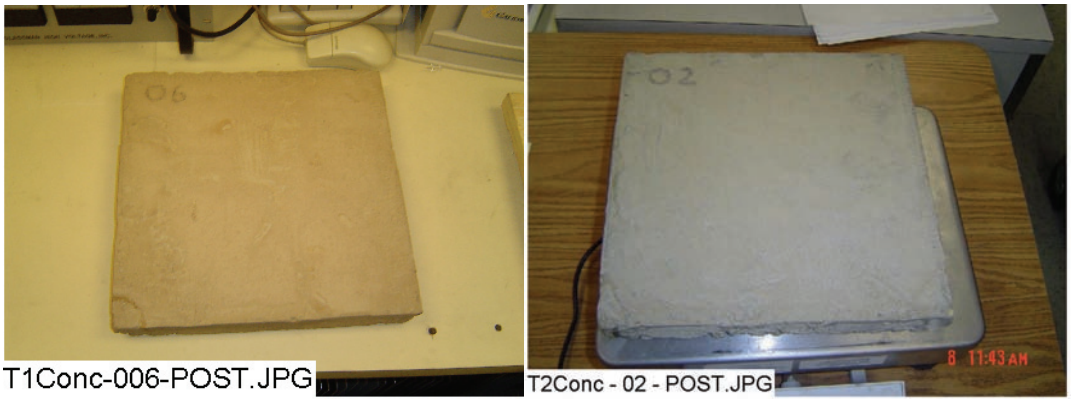

Figure 4-119. ICET Test #1 Conc-6 submerged, post-test (left); ICET Test #2 Conc-2 submerged, post-test (right).

Figure 4-120. ICET Test #3 Conc-5 submerged, post-test (left); ICET Test #4 Conc-4 submerged, post-test (right).

Figure 4-121. ICET Test #5 Conc-003 submerged, post-test.

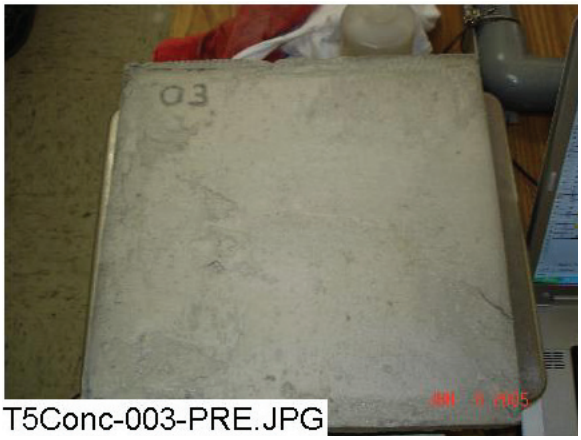

Figure 4-122. Unused concrete coupon.

Overall, the Test #4 environment resulted in less significant changes to the submerged coupon appearance.

Table 4-9 displays the mean weight gain/loss summary in grams for all of the submerged coupons.

Table 4-9. Mean Weight Gain/Loss Data for Submerged Coupons (g)

	Test Number				
Coupon Type	**1**	**2**	**3**	**4**	**5**
CU	0.1	<0.1	0.3	0.2	–0.2
IOZ	3.1	3.8	1.8	2.3	1.6
GS	0.0	28.6	15.0	0.3	0.1
AL	–98.6	–0.9	0.6	0.0	–11.2
US	–23.3	1.4	–1.1	0.2	0.0
Concrete	233.0	240.7	180.5	239.6	225.9

The submerged concrete samples' mean weight gain ranged from 180 to 241 g. Much of that weight gain is attributed to retained water in the samples. It is interesting to note that the weight

gains for Tests #1, #2, #4, and #5 were similar, while the Test #3 weight gain was 45–60 g less. It is possible that water retention was impeded by the Test #3 surface coating (Figure 4-120). The mean weight gain/loss of the submerged carbon steel (uncoated steel, US) coupons did not exceed 1.5 g, with the exception of the Test #1 coupon, which lost approximately 23 g. The aluminum coupons in Tests #1 and #5 lost significant weight, about 25% and 3% of their pretest weights, respectively. There were no significant weight changes in the aluminum coupons in the other tests. The submerged galvanized steel coupons in Tests #2 and #3 experienced mean weight gains of approximately 3% and 1.5% of their pre-test values, respectively. Tests #1, #4, and #5 coupons exhibited insignificant weight changes. The mean weight gain of the submerged inorganic-zinc-coated steel coupons ranged from 1.6 to 3.8 g. The submerged copper coupons experienced mean weight differentials that did not exceed 0.5 g.

Unsubmerged Coupons

Figures 4-123 through 4-125 are post-test pictures of unsubmerged aluminum coupons from each test. Each post-test photograph depicts coupons that were loaded in Rack 2 (see Figure 2-2), which was in the southern position of the middle tier of the tank. Using the same rack location facilitates direct comparison of aluminum coupons from each test. Each post-test aluminum coupon exhibits a similar vertical, streak pattern of white deposits. The deposit concentration was also similar for all of the displayed coupons. Each coupon is predominantly dull gray, with a tint of reddish-brown visible on the coupons from Tests #1, #4, and #5.

Figure 4-123. Test #1 Al-42 unsubmerged (left); Test #2 Al-101 unsubmerged (right).

Figure 4-124. Test #3 Al-159 unsubmerged (left); Test #4 Al-3 unsubmerged (right).

Figure 4-125. Test #5 Al-247 unsubmerged.

Figures 4-126 through 4-128 are post-test pictures of unsubmerged galvanized steel coupons from each test. Each post-test photograph depicts coupons that were loaded in Rack 3, which was in the center position of the middle tier of the tank (Figure 2-2). The concentration and pattern of deposition on the Tests #1 and #2 coupons are similar. The deposition patterns exhibited by these coupons are a combination of faint white steaks and small white clusters located in random locations. There are much fewer deposits on the Tests #3, #4, and #5 coupons. Each coupon is predominantly gray to silver, which is consistent with its original color (Figure 4-106).

Figure 4-126. Test #1 GS-223 unsubmerged (left); Test #2 GS-366 unsubmerged (right).

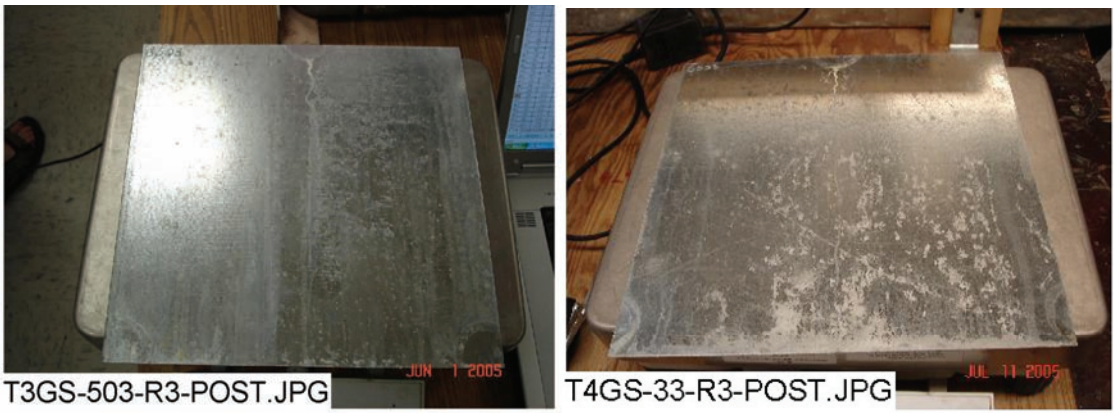

Figure 4-127. Test #3 GS-503 unsubmerged (left); Test #4 GS-33 unsubmerged (right).

Figure 4-128. Test #5 GS-167 unsubmerged.

Figures 4-129 through 4-131 are post-test pictures of unsubmerged copper coupons from each test. Each post-test photograph depicts coupons that were loaded in rack #7, which was in the northern position of the top tier of the tank (Figure 2-2). The pattern of deposition for each coupon is similar and consists of faint white, vertical streaks. The depositions on the Tests #1 and #5 coupons are the least concentrated. The deposition concentration on the remaining coupons is similar. Each coupon is predominantly reddish-brown, which is consistent with their original color (Figure 4-114).

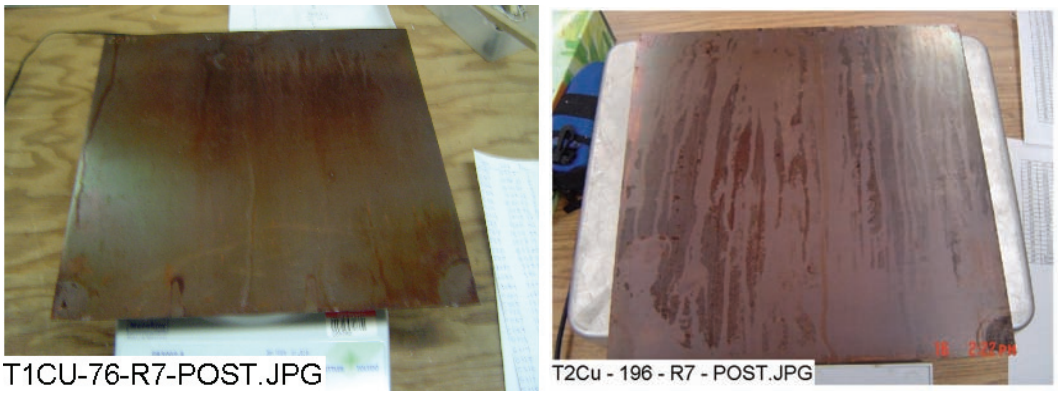

Figure 4-129. Test #1 CU-76 unsubmerged (left); Test #2 CU-196 unsubmerged (right).

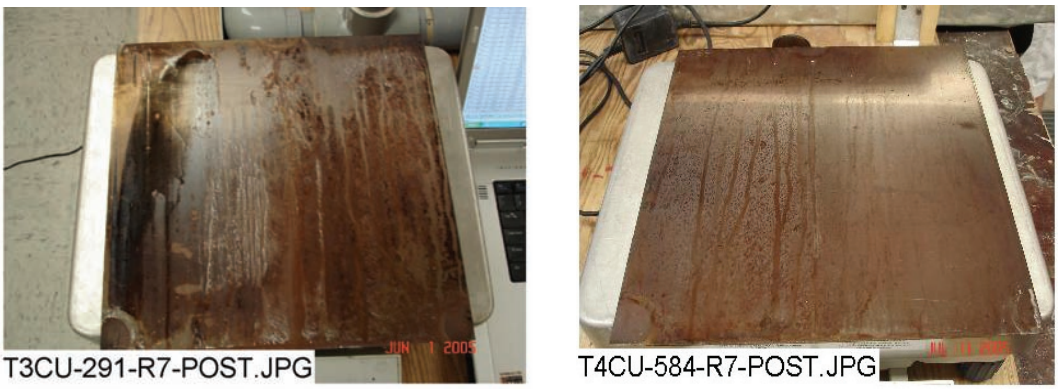

Figure 4-130. Test #3 CU-291 unsubmerged (left); Test #4 CU-584 unsubmerged (right).

Figure 4-131. Test #5 CU-587 unsubmerged.

Figures 4-132 through 4-134 are post-test pictures of unsubmerged inorganic zinc-coated steel coupons from each test. Each post-test photograph depicts coupons that were loaded in Rack 5, which was in the southern position of the top tier of the tank. The pattern of deposition for Tests #1, #2, #4, and #5 coupons consists of lightly-concentrated, white clusters. The Test #3 coupon depositions consist of vertical streaks that are mainly congregated near the right-hand-side coupon edge. Each coupon is predominantly dull gray, which is consistent with its original appearance (Figure 4-110).

Figure 4-132. Test #1 IOZ-48 unsubmerged (left); Test #2 IOZ-26 unsubmerged (right).

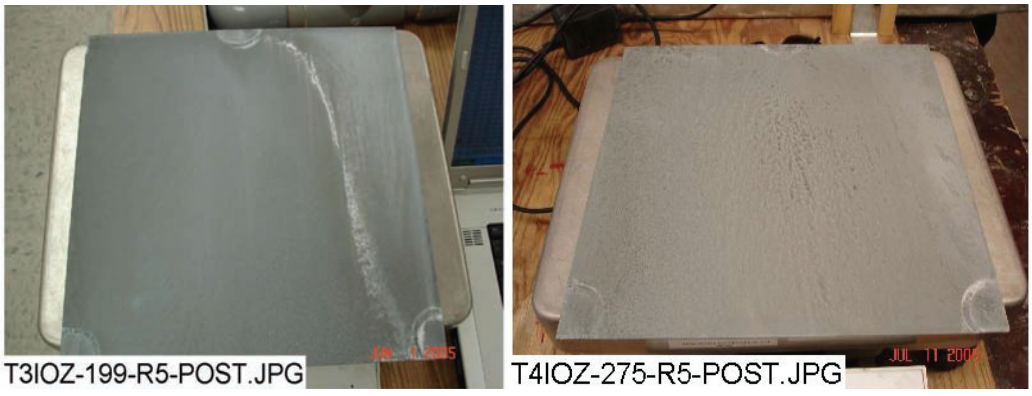

Figure 4-133. Test #3 IOZ-199 unsubmerged (left); Test #4 IOZ-275 unsubmerged (right).

Figure 4-134. Test #5 IOZ-356 unsubmerged.

Figures 4-135 through 4-137 are post-test pictures of unsubmerged uncoated carbon steel coupons from each test. Each post-test photograph depicts coupons that were loaded in Rack 6, which was in the center of the top tier of the tank (Figure 2-2). The deposits for each coupon consist of reddish-brown rust. However, the concentration of rust varies between tests. The concentration of the Tests #2 and #3 coupons is significant and covers nearly the entire surface of each coupon. The coupons from Tests #1, #4, and #5 exhibit sparsely concentrated, rust-like splotches. Each coupon is predominantly dull silver, close to its original color (Figure 4-118).

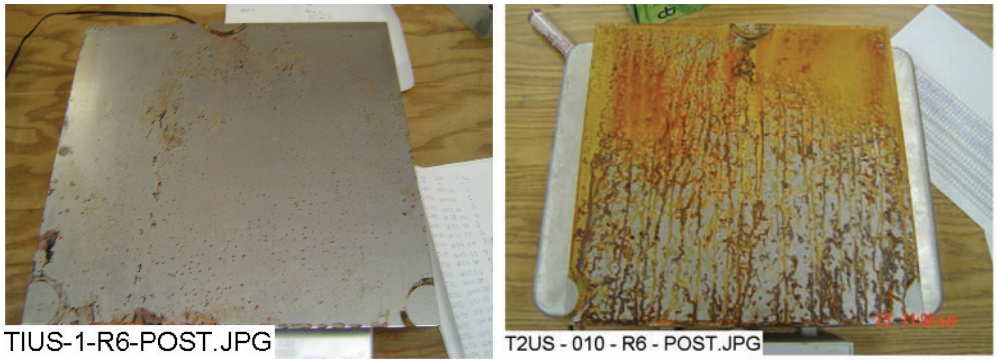

Figure 4-135. Test #1 US-1 unsubmerged (left); Test #2 US-10 unsubmerged (right).

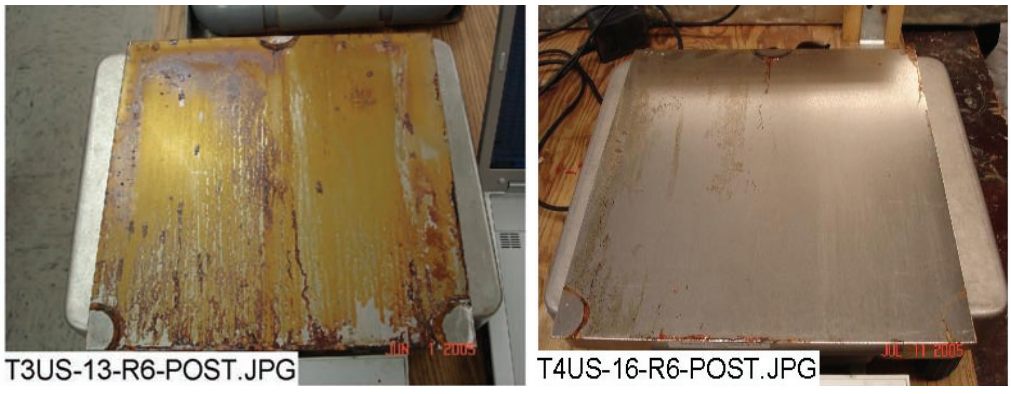

Figure 4-136. Test #3 US-13 unsubmerged (left); Test #4 US-16 unsubmerged (right).

Figure 4-137. ICET Test #5 US-18 unsubmerged.

Table 4-10 displays the mean gain/loss summary in grams for all of the unsubmerged coupons.

Table 4-10. Mean Gain/Loss Data for Unsubmerged Coupons (g)

	Test Number				
Coupon Type	**1**	**2**	**3**	**4**	**5**
CU	–0.2	<0.1	0.2	0.3	0.2
IOZ	1.2	1.7	2.0	1.1	1.2
GS	0.0	0.4	0.2	0.2	0.2
AL	0.7	0.4	0.4	0.6	0.4
US	0.0	1.3	1.0	–0.4	0.2

The mean weight differentials for unsubmerged coupons are more consistent among the tests, and there are no weight gains or losses as significant as with some of the submerged coupons. The copper samples experienced mean weight changes ranging from <0.1 to 0.3 g. The range of mean weight gain for the inorganic-zinc-coated steel coupons was 1.1 to 2.0 g. The galvanized steel coupons' mean weight gain ranged from 0.0 to 0.4 g. The aluminum coupons' mean weight gain ranged from 0.4 to 0.7 g. The range of mean weight gain/loss for the carbon steel coupons was 0 to 1.3 g.

4.4.2. SEM/EDS

The surface and the morphology of metal coupons were altered by corrosion because of exposure to the test solutions, condensate, or sprays during the ICET tests. The extent of corrosion on different coupons depended on the metals and solution chemistry of each individual test, such as pH and type of insulation material (fiberglass or cal-sil). Table 4-11 lists the redox potential (Ref. 9) of the metals on the coupon surfaces. The more negative the redox potential the more likely it is that the metal will oxidize and corrode. From Table 4-11, aluminum is the metal most likely to corrode, followed by zinc, iron, and copper. It should be noted that passivation layers (such as aluminum silicate) may impede the corrosion process independent of the redox potential (see Section 4.4.3). This type of passivation may be more significant in the tests with cal-sil, which can release a significant amount of calcium and silica to solution. The data of coupon

weight gain/loss after the tests do not necessarily correlate with the amount of corrosion because weight loss caused by corrosion can be offset by weight gain caused by the deposition of corrosion products on the coupon surface. In addition to redox potential and passivation layers, solution chemistry also affects the corrosion. For example, the solubility of aluminum species is higher at pH 9 than at pH 7; therefore, the corrosion is more severe at pH 9.

Table 4-11. Standard Redox Potential of the Metals Used in the ICET Tests

Metals	Reactions	Redox Potential (E^0/V)
Aluminum	$Al^{3+} + 3e^- \leftrightarrow Al$	–1.662
Copper	$Cu^{2+} + 2e^- \leftrightarrow Cu$	0.3419
Iron	$Fe^{3+} + 3e^- \leftrightarrow Fe$	–0.037
Zinc	$Zn^{2+} + 2e^- \leftrightarrow Zn$	–0.7618

Submerged Metal Coupons

During the ICET tests, trace metal cations may be released from the submerged metal coupon surfaces because of corrosion. Subsequently, the released metal cations may form complexes with the anions from the solution, such as OH^-, SiO_3^{2-}, and CO_3^{2-}. In addition, the complexed anions may attract other cations from the solution, such as Ca^{2+}, Mg^{2+}, Al^{3+}, Cu^{2+}, Zn^{2+}, and H^+. As a result, corrosion products (deposits) may form and continuously grow on the metal coupon surfaces. The adherence between the metal coupons and the deposits is through chemical bonds, which are much stronger than van der Waals forces. Because of the vertical orientation of the metal coupons in the tank (with a small horizontal cross-sectional area), the deposits on the metal coupon surface are likely of chemical origin rather than being the result of particles settling on the surface. Corrosion also may cause pitting of the coupon surfaces. As a result, a rougher coupon surface was often observed as compared with the unused coupons.

Based on SEM/EDS results, the dominant corrosion products on the submerged aluminum coupons appear to be aluminum hydroxide, with other substances containing silicon, calcium, oxygen, and carbon also present. On the submerged copper coupons, the possible corrosion products include CuO, $Cu_2(CO_3)(OH)_2$, and substances containing calcium, silicon, aluminum, and oxygen. On the submerged galvanized steel coupons, the possible corrosion products are oxides, hydroxides, silicates, and carbonate compounds of zinc, calcium, and aluminum. On the submerged steel coupon, the possible corrosion products include oxide, hydroxide, silicate, and carbonate compounds of iron and calcium and compounds composed of iron, silicon, calcium, and aluminum. Because of the differences of specific chemicals used in each test, some specific deposits were found on submerged metal coupons. For example, because TSP was used in Test #2, phosphate-related deposits were found on the submerged copper, galvanized steel, and uncoated steel coupons. (Phosphate was mainly precipitated out by calcium as gel-like material in Test #3). The introduction of cal-sil in Tests #3 and #4 caused silicate passivation on submerged aluminum coupon surfaces (see Section 4.4.3).

Unsubmerged Metal Coupons

The unsubmerged coupons were affected by the test solution only during the 4-hour spray phase on the first day of the test and, following that, were affected by condensation throughout the test.

Compared to the submerged coupons, the unsubmerged coupons had limited contact with the test solution; thus, the effect of solution chemistry on corrosion was limited. This effect may decrease the degree of corrosion on the unsubmerged coupons. However, the unsubmerged coupons have more contact with moist air and oxygen than the submerged coupons. As a result, oxygen had a greater chance to oxidize the coupons. The relative degree of corrosion on the unsubmerged coupons depended on these two competitive processes. If the physical and chemical changes that the unsubmerged coupons experienced during the ICET tests were less significant than the changes on the submerged coupons, the solution chemistry was the limiting step for corrosion on unsubmerged coupons. Otherwise, the oxidation process by oxygen from air was important for corrosion of the unsubmerged coupons. For unsubmerged coupons, it should be noted that the initial corrosion caused by the test solution during the 4-hour spray period may affect their consequent corrosion in moist air, because the test solution may damage the passivation oxide layer on the surface of the coupons, such as aluminum (Ref. 10) and zinc (Ref. 11).

Based on SEM/EDS results, the dominant corrosion products on the unsubmerged aluminum coupons appear to be aluminum hydroxide and/or aluminum oxide, and other corrosion products containing silicon, calcium, oxygen, and carbon also exist. On the unsubmerged copper coupons, the corrosion products are likely to be CuO. The corrosion products were composed of carbon, oxygen, calcium, silicon, and chlorine on the unsubmerged galvanized steel coupon surface. On the unsubmerged steel coupons, the likely corrosion products are Fe_2O_3, $Fe(OH)_3$, and $Fe_2(CO_3)_3$.

Submerged Aluminum Coupons

Figures 4-138 through 4-140 are the SEM images of unused and submerged aluminum coupons from Tests #1 through #5, respectively. As discussed previously, the coupon surface becomes very rough after the tests. Because of the negative redox potential of aluminum and high pH value (~9.5) in Test #1, the most severe corrosion of aluminum occurred in Test #1. The aluminum concentration reached ~380 mg/L in the Test #1 solution. The Test #5 aluminum coupons also experienced significant corrosion, although less than in Test #1. Test #5 was the only other test (besides Test #1) to have a significant aluminum concentration, which rose to about 50 mg/L in the test solution.

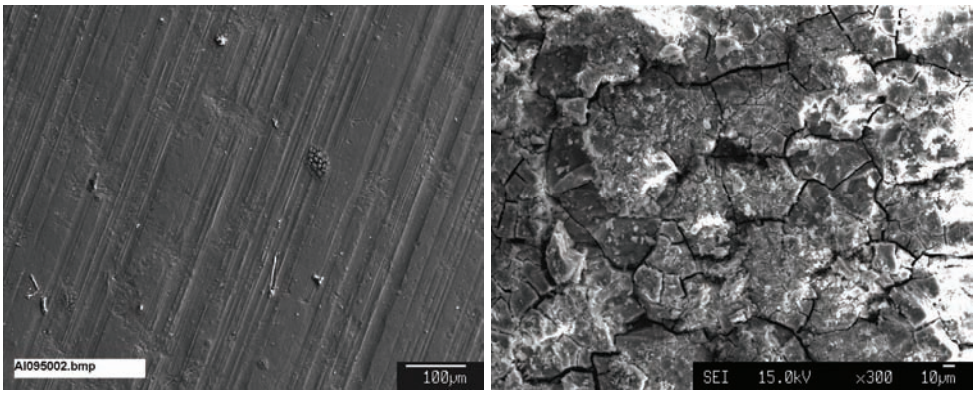

Figure 4-138. Unused aluminum coupon (left); Test #1 submerged aluminum coupon (right).

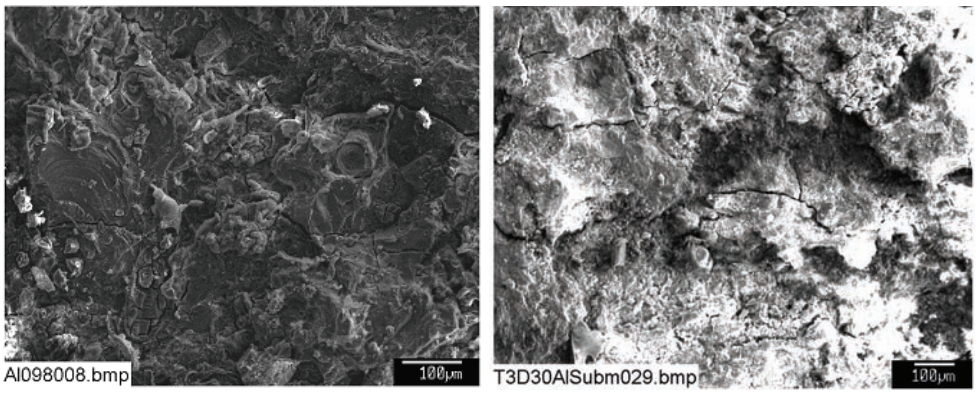

Figure 4-139. Test #2 submerged aluminum coupon (left); Test #3 submerged aluminum coupon (right).

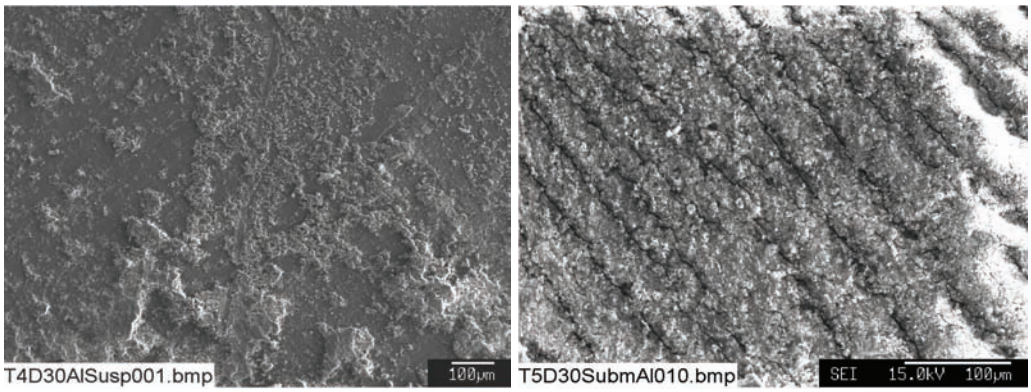

Figure 4-140. Test #4 submerged aluminum coupon (left); Test #5 submerged aluminum coupon (right).

Unsubmerged Aluminum Coupons

As shown in Figures 4-141 through 4-143, corrosion still occurred on the unsubmerged aluminum coupons because the coupons were affected by the test solution during the 4-hour spray period on the first day of the tests and by the moist air throughout the tests. However, the degree of corrosion apparently is less severe than on the submerged coupons because of limited contact with the liquid and, thus, there is limited mass transfer of the corrosion products and ionic species.

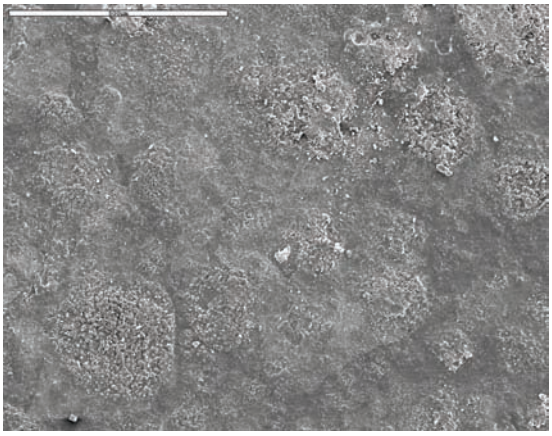

Figure 4-141. Test #1 unsubmerged aluminum.

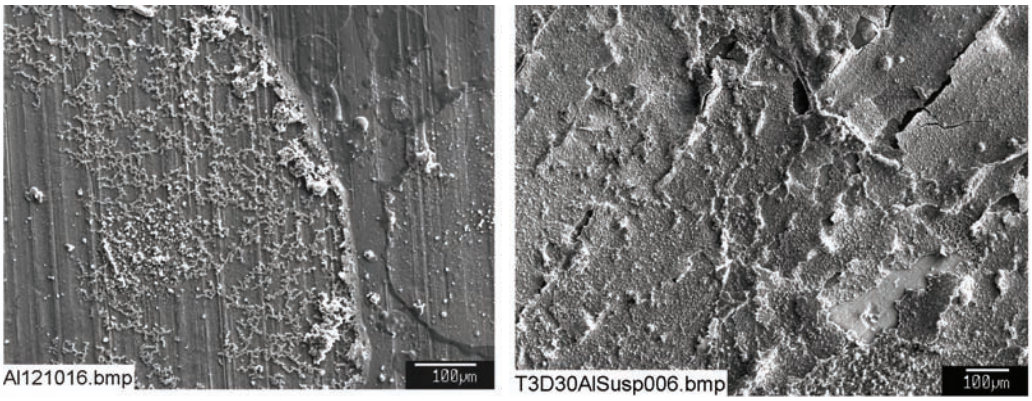

Figure 4-142. Test #2 unsubmerged aluminum (left); Test #3 unsubmerged aluminum (right).

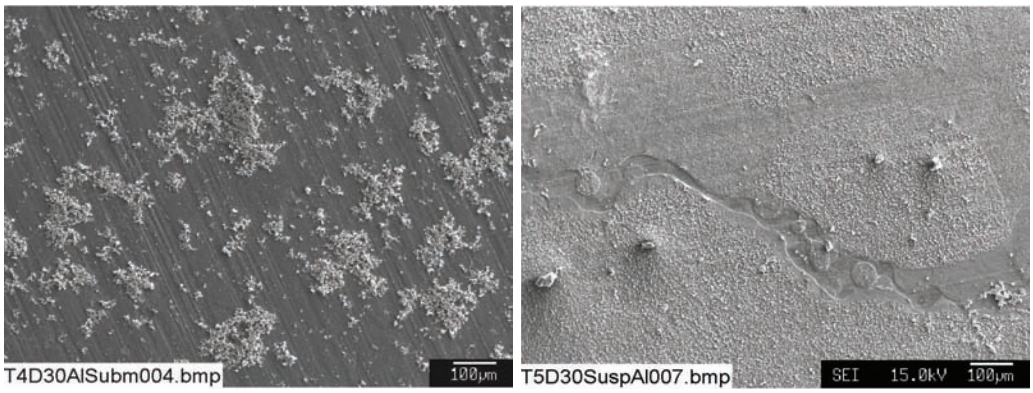

Figure 4-143. Test #4 unsubmerged aluminum (left); Test #5 unsubmerged aluminum (right).

Submerged Copper Coupons

Figures 4-144 through 4-146 show SEM images of unused and submerged copper coupons from Tests #1 through #5, respectively. As discussed previously, the coupon surface became significantly rougher after the tests. Because of the positive redox potential of copper, the corrosion of copper was less significant than the corrosion of aluminum. The copper concentration was less than 1.2 mg/L in all five of the tests, although the copper concentration may have been affected by other chemical species in the solution that complexed with copper and form precipitates.

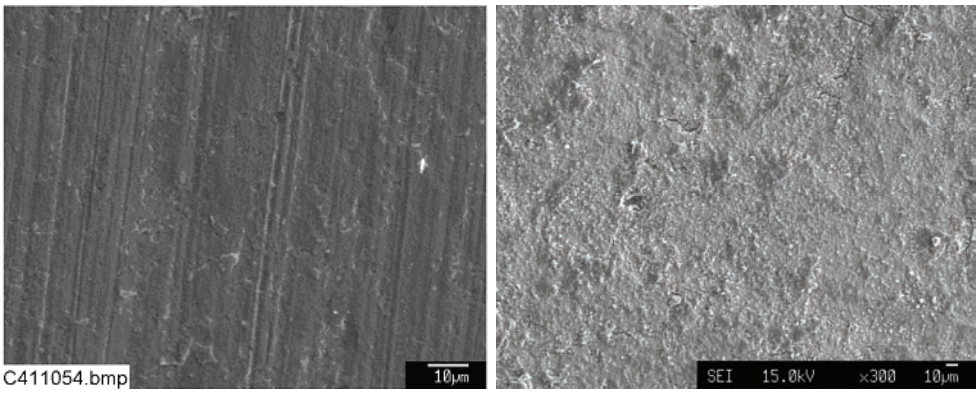

Figure 4-144. Unused copper coupon (left); Test #1 submerged copper coupon (right).

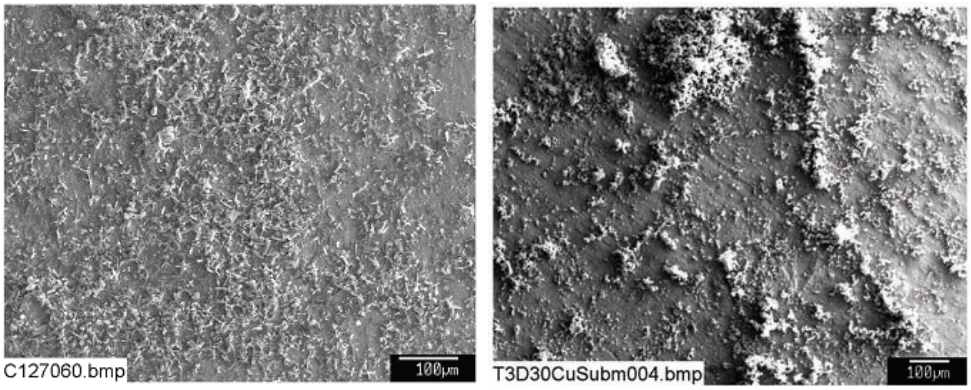

Figure 4-145. Test #2 submerged copper coupon (left); Test #3 submerged copper coupon (right).

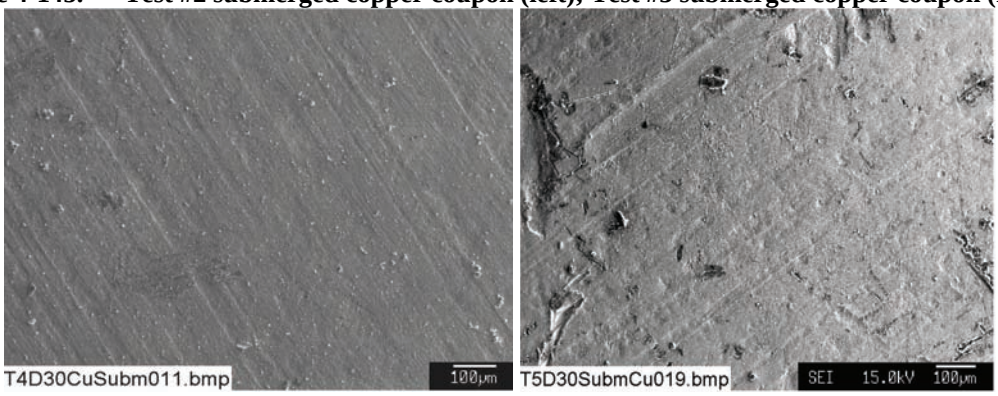

Figure 4-146. Test #4 submerged copper coupon (left); Test #5 submerged copper coupon (right).

Unsubmerged Copper Coupons

As shown in Figures 4-147 through 4-149, limited corrosion occurred on the unsubmerged copper coupons. The coupons were affected by the test solution only during the 4-hour spray period on the first day of the tests and by the moist air throughout the tests. As discussed previously, the degree of corrosion was significantly less than on the submerged copper coupons because of the limited mass-transfer process.

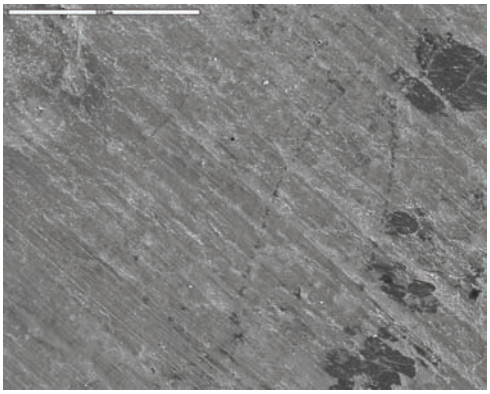

Figure 4-147. Test #1 unsubmerged copper.

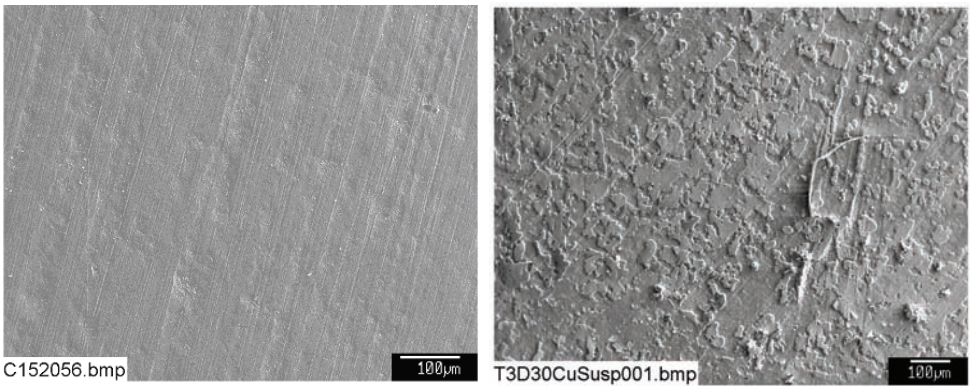

Figure 4-148. Test #2 unsubmerged copper (left); Test #3 unsubmerged copper (right).

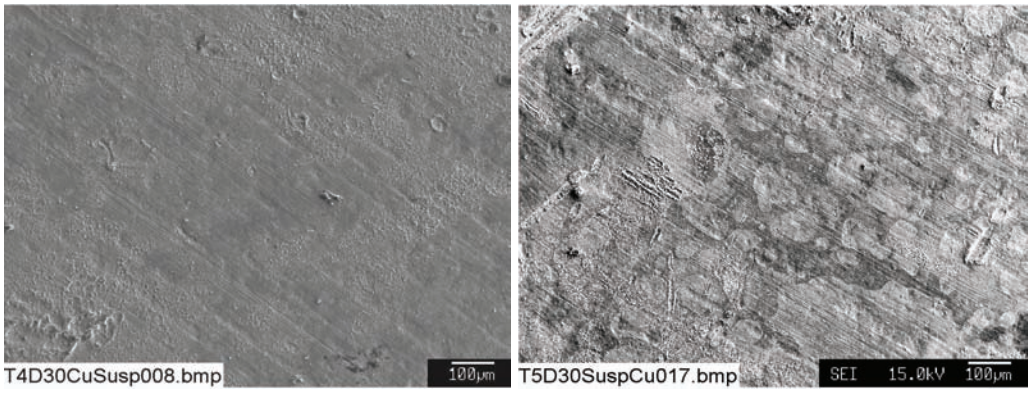

Figure 4-149. Test #4 unsubmerged copper (left); Test #5 unsubmerged copper (right).

Submerged Galvanized Steel Coupons

Figures 4-150 through 4-152 show SEM images of unused and submerged GS coupons from Tests #1 through #5, respectively. For the GS coupons, the steel surface is coated with zinc. Zinc has the second lowest redox potential, as shown in Table 4-9. The purpose of zinc galvanization is to coat iron with a material that is more likely to corrode; therefore, the corrosion of iron is prevented by the corrosion of the zinc. As a result, the corrosion of the zinc surface layer causes the coupon surface to become significantly rougher after the tests. It should be noted that the zinc

concentration was <10 mg/L in all five of the tests, which was higher than copper but generally lower than aluminum, in accordance with the redox potential. It should be noted that the zinc concentration in solution may have been affected by other chemical species that complexed with zinc and formed precipitates.

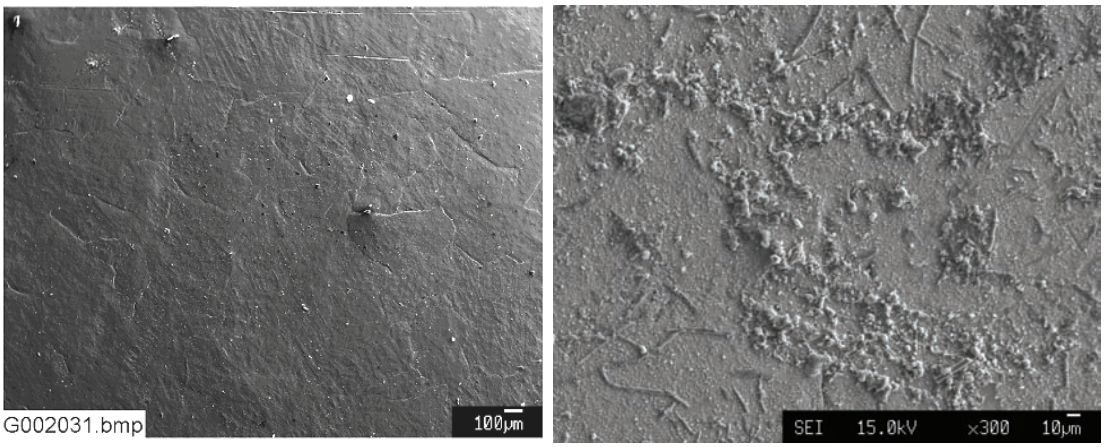

Figure 4-150. Unused galvanized steel coupon (left); Test #1 submerged galvanized steel (right).

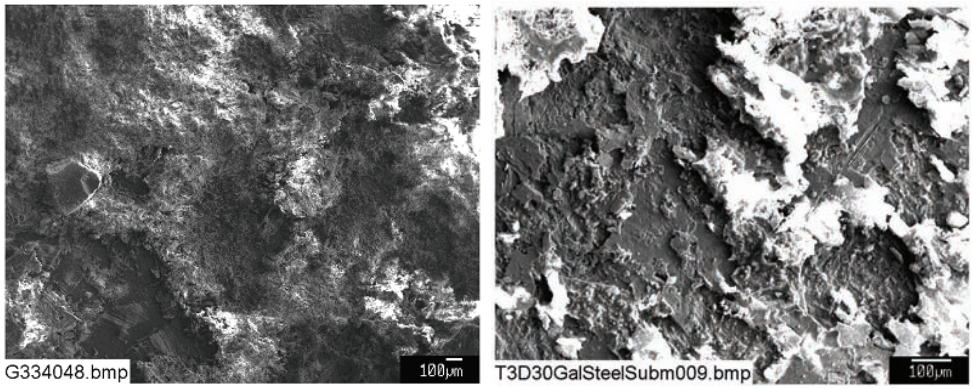

Figure 4-151. Test #2 submerged galvanized steel (left); Test #3 submerged galvanized steel (right).

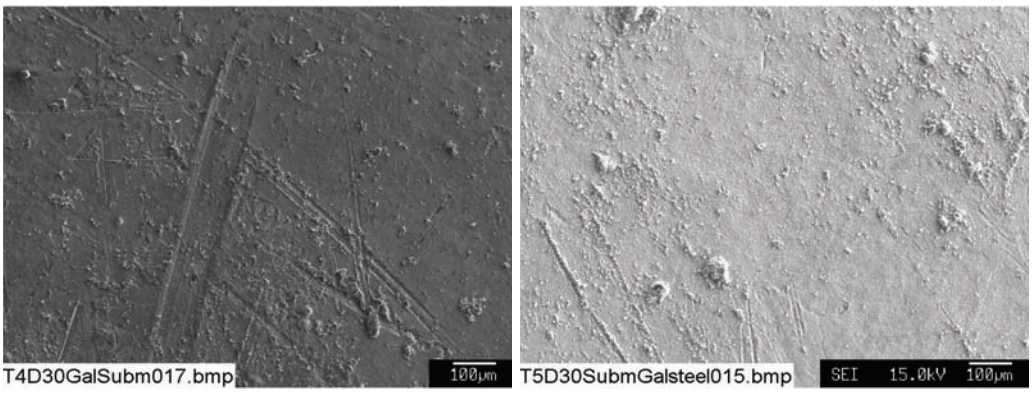

Figure 4-152. Test #4 submerged galvanized steel (left); Test #5 submerged galvanized steel (right).

Unsubmerged Galvanized Steel Coupons

As shown in Figures 4-153 to 4-155, corrosion occurred on the unsubmerged GS coupons. However, in contrast to the aluminum and copper coupons, the amount of corrosion on the unsubmerged GS coupons was not always less than on the submerged coupons. The possible reason is that oxygen from air oxidized the unsubmerged GS surfaces to a large degree.

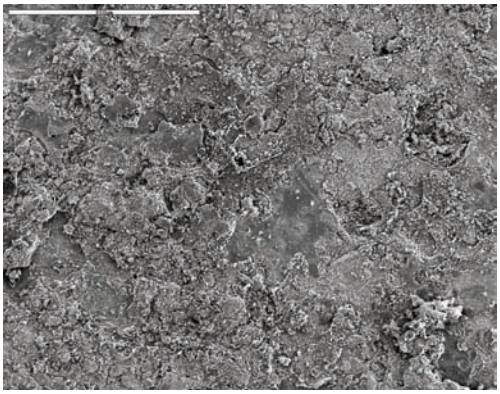

Figure 4-153. Test #1 unsubmerged galvanized steel.

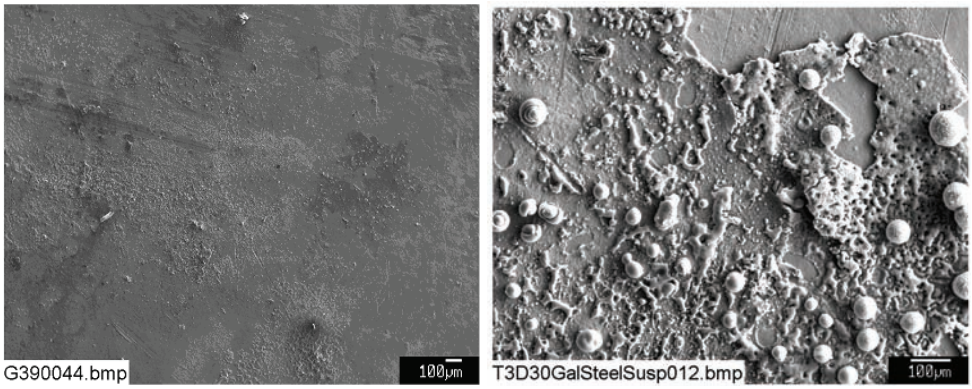

Figure 4-154. Test #2 unsubmerged galvanized steel (left); Test #3 unsubmerged galvanized steel (right).

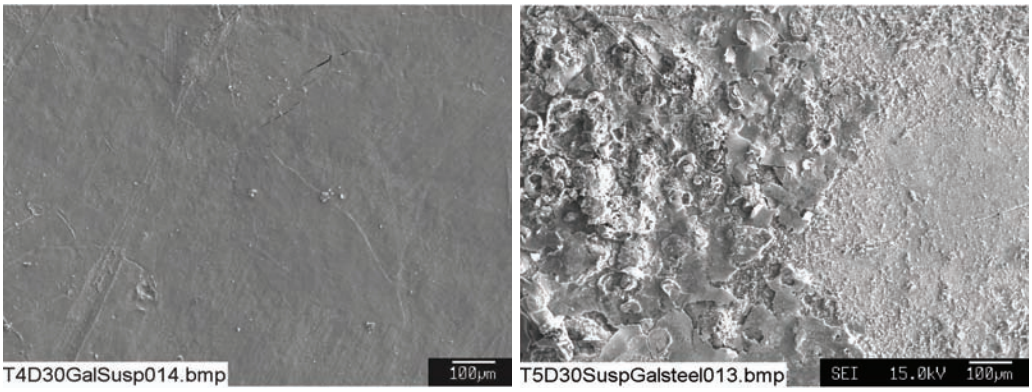

Figure 4-155. Test #4 unsubmerged galvanized steel (left); Test #5 unsubmerged galvanized steel (right).

Submerged Carbon Steel Coupons

Figures 4-156 to 4-158 are SEM images of unused and submerged carbon steel coupons from Tests #1 through #5, respectively. Iron has the second highest redox potential of the metals shown in Table 4-9. Therefore, iron is more readily oxidized than copper. As a result, corrosion was more significant with iron than with copper, based on the SEM images, i.e., the coupon surface became rough after the tests. However, the iron concentration in solution was mostly less than the detection limit in the ICET tests. The reason for the low iron concentration is that the product of iron corrosion, ferric hydroxide (rust), is extremely insoluble over the pH range of these tests and rust will form at the surface of the coupon instead of releasing soluble ferric ions into solution.

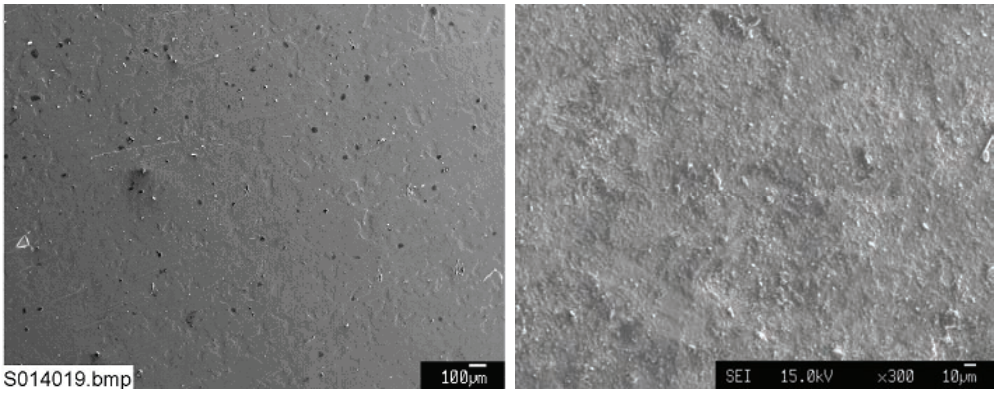

Figure 4-156. Unused carbon steel coupon (left); Test #1 submerged carbon steel (right).

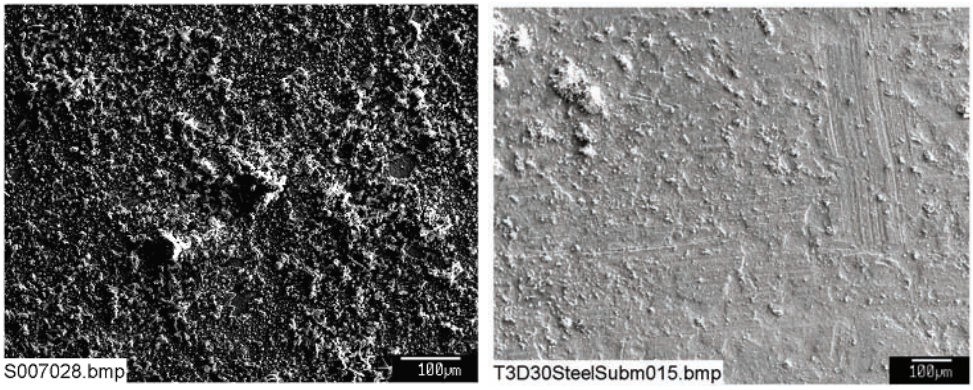

Figure 4-157. Test #2 submerged carbon steel (left); Test #3 submerged carbon steel (right).

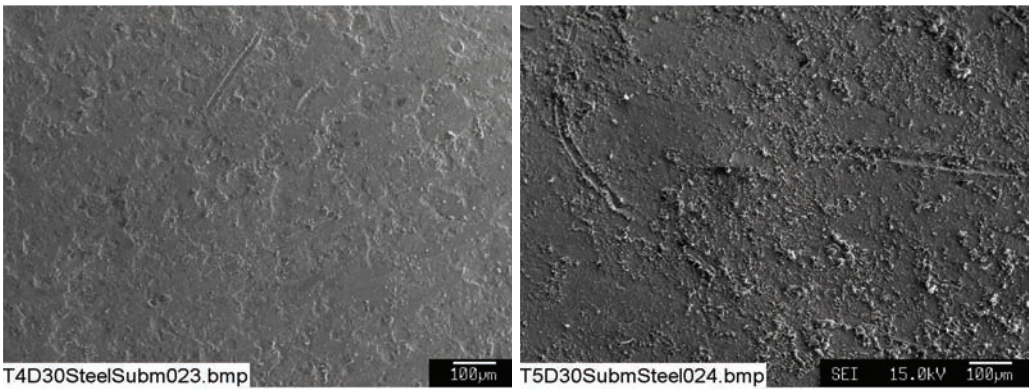

Figure 4-158. Test #4 submerged carbon steel (left); Test #5 submerged carbon steel (right).

Unsubmerged Carbon Steel Coupons

As shown in Figures 4-159 to 4-161, corrosion also occurred on the unsubmerged carbon steel coupons. As with the galvanized steel coupons, the degree of corrosion was not always greater for the submerged carbon steel coupons, especially for Tests #3 and #5. In those tests, the carbon steel corrosion rates in the moist oxygenated spray zone environment appeared to be greater than the submerged coupons.

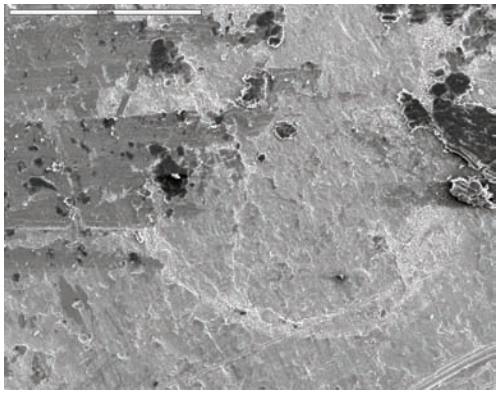

Figure 4-159. Test #1 unsubmerged carbon steel.

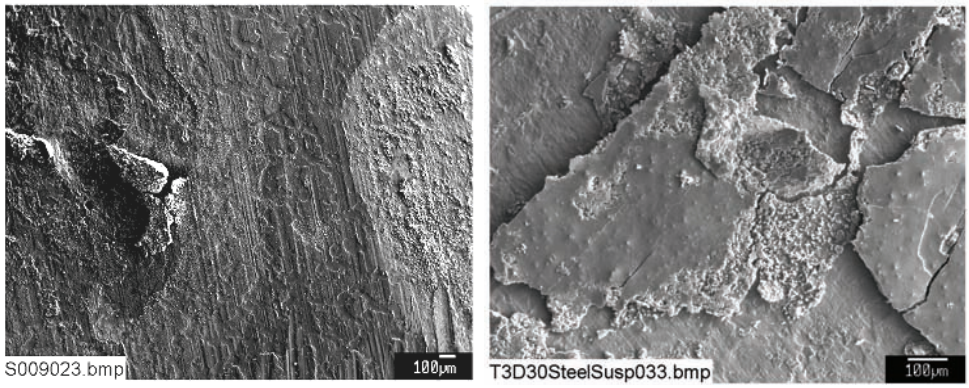

Figure 4-160. Test #2 unsubmerged carbon steel (left); Test #3 unsubmerged carbon steel (right).

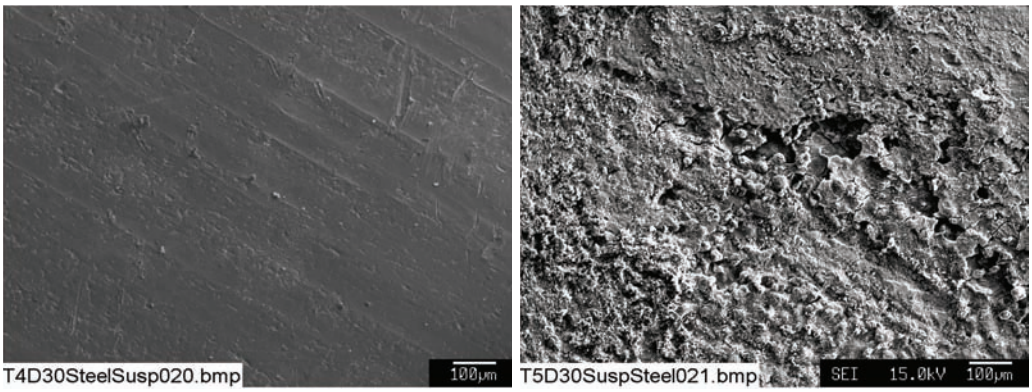

Figure 4-161. Test #4 unsubmerged carbon steel (left); Test #5 unsubmerged carbon steel (right).

4.4.3. Passivation of Test #4 Submerged Al Coupons

An interesting observation in the ICET tests is that the Test #4 submerged aluminum coupons had significantly less corrosion than the aluminum coupons in Test #1. The aluminum coupons (with an average weight of 392.0 g) had an average weight loss of 98.6 g over 30 days in Test #1 compared to an average weight loss of <0.1 g over 30 days in Test #4. The initial solution chemistry of these two tests was nearly identical, so the initial expectation was that the corrosion rates would be similar in both tests. The primary difference between the two tests was the insulation material; the Test #1 insulation was 100% fiberglass, and the Test #4 insulation was 20% fiberglass and 80% cal-sil. Since cal-sil was the only component that was in Test #4 and not in Test #1, it is possible that the cal-sil contributed to the critical difference in solution chemistry that prevented corrosion of the aluminum coupons in Test #4. Additional insights on the differences in aluminum corrosion in these tests can be found in Ref. 12.

Experimental results indicated differences in some aqueous concentrations over the duration of Tests #1 and #4. As shown in Figure 4-162, the aluminum concentration in Test #1 started at ~50 mg/L, increased until Day 16, and leveled off at ~350 mg/L, after Day 18. In contrast, the aluminum concentration in Test #4 was measured near the detection limit on the first 2 days and stayed below the detection limit for the remainder of the test. The increase in aluminum concentration over the first half of Test #1 suggests that corrosion proceeded over a number of days but stopped because the surface of the coupon was passivated and additional corrosion was impeded. Thus, it is likely that the differences in corrosion were because of differences in passivation of the coupon surfaces. Bench-scale experimentation and modeling verified that the solubility limit of aluminum at this pH and temperature was above the observed steady state concentration. Therefore, the leveling-off of aluminum concentration in Test #1 was not because of solubility considerations.

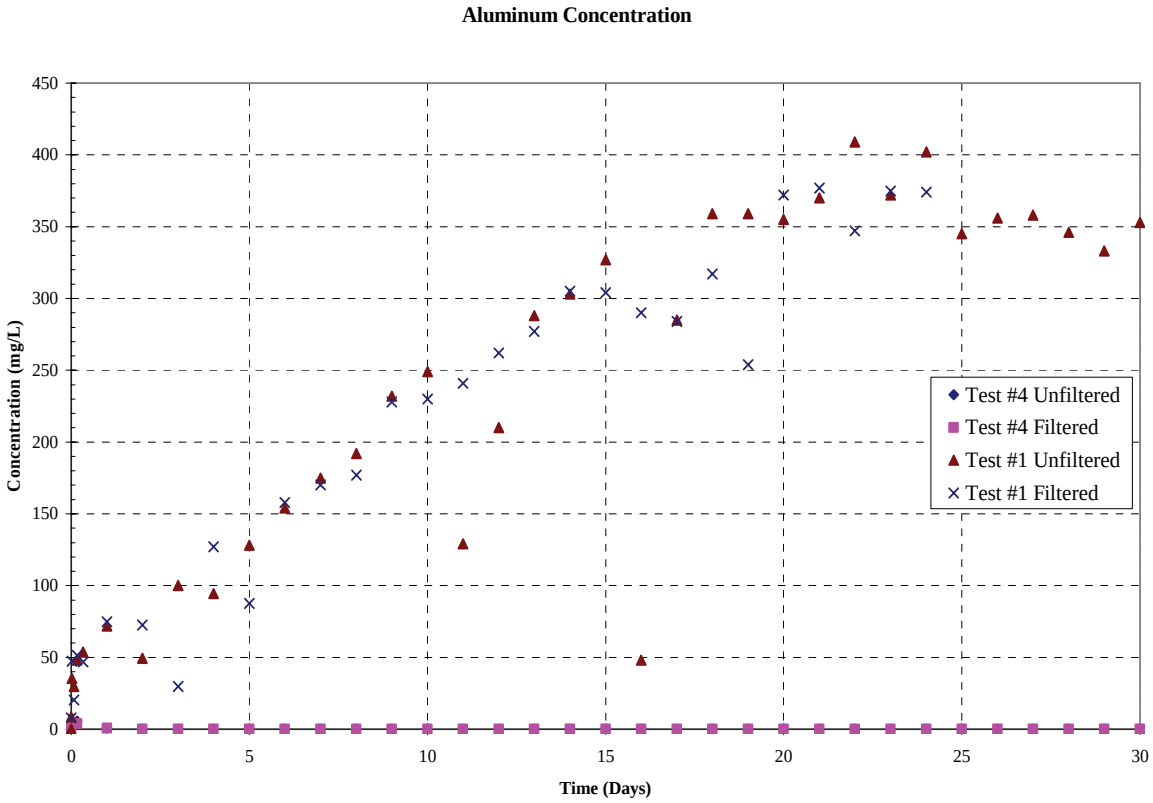

Figure 4-162. Aluminum concentration in ICET Test #1 and Test #4 daily water samples.

Figure 4-163 indicates that the silica concentration in the Test #4 solution was about one order of magnitude higher than in Test #1. The higher silica concentration was likely because of dissolution of cal-sil and the release of silicate to the solution in Test #4. A result may have been a reaction that formed an insoluble aluminum silicate coating on the coupons. To investigate this possibility, SEM and EDS analyses were performed on the Test #1 and #4 aluminum coupons. SEM images of an aluminum coupon after 30 days of submersion in Test #4 are shown in Figures 4-164 and 4-165, and EDS analyses associated with this coupon are shown in Figures 4-166 and 4-167. The SEM images show the formation of a crystalline material on the surface of the aluminum coupons, and the EDS in Figure 4-166 indicates that the major components on this crystalline structure were aluminum, oxygen, silicon, sodium, and calcium, with small amounts of carbon and magnesium. In contrast, the EDS of regions that appear to be the original coupon surface shows that the material was composed primarily of aluminum and oxygen, with small amounts of silicon and sodium. The difference in elemental composition of these two locations is compared in Table 4-12. The amount of oxygen in the area that appears to be the original surface may be an aluminum oxide or aluminum hydroxide surface layer. Aluminum oxide is very effective at passivating aluminum in air but may be less effective at passivating aluminum in aqueous solutions similar to those found in the ICET tests.

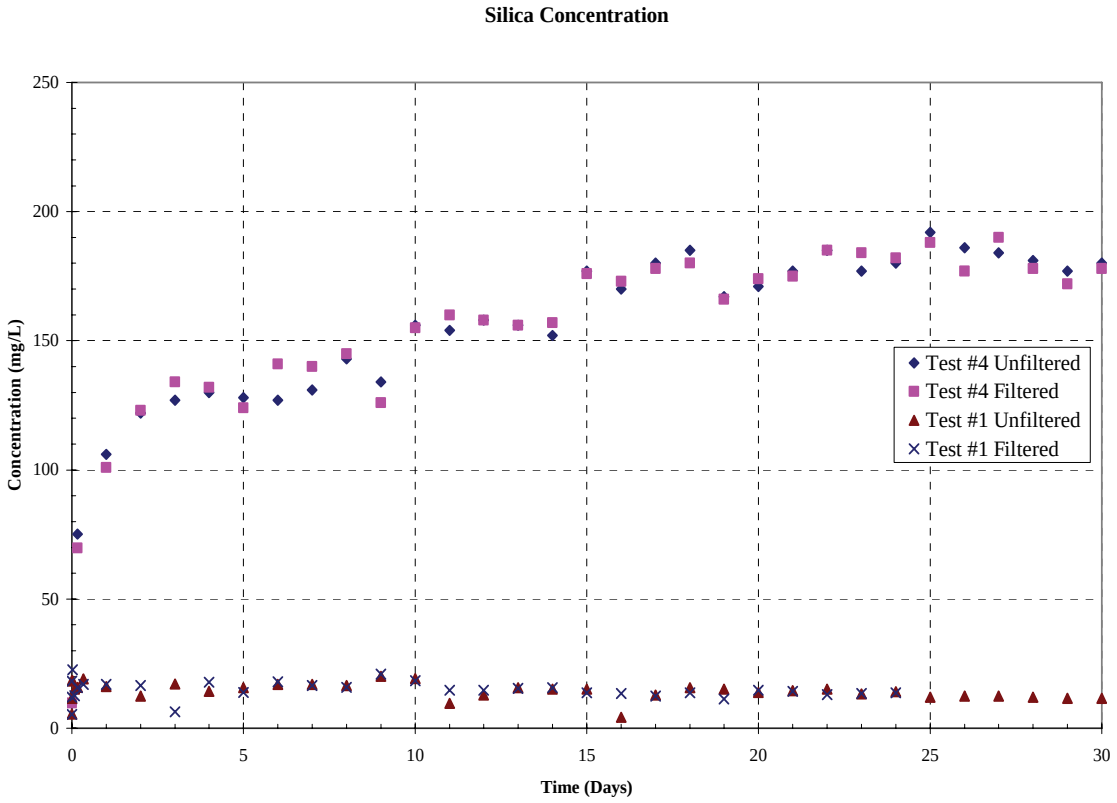

Figure 4-163. Silica concentration in ICET Test #1 and Test #4 daily water samples.

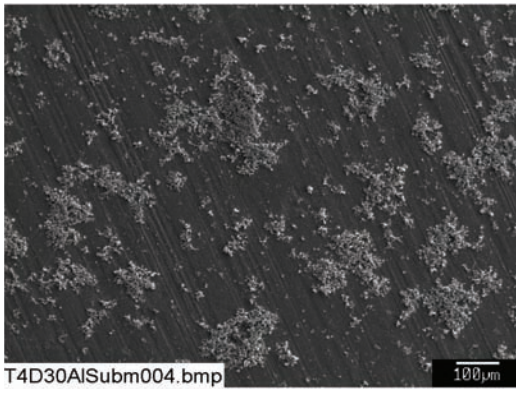

Figure 4-164. SEM image, magnified 100 times, of a Test #4, Day 30, submerged aluminum coupon sample. (T4D30AlSubm004.bmp)

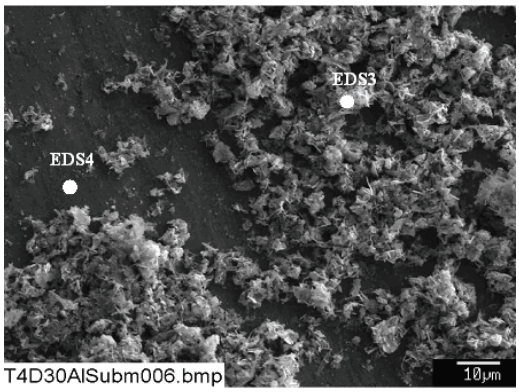

Figure 4-165. Annotated SEM image, magnified 1000 times, of a Test #4, Day 30, submerged aluminum coupon sample. (T4D30AlSubm006.bmp)

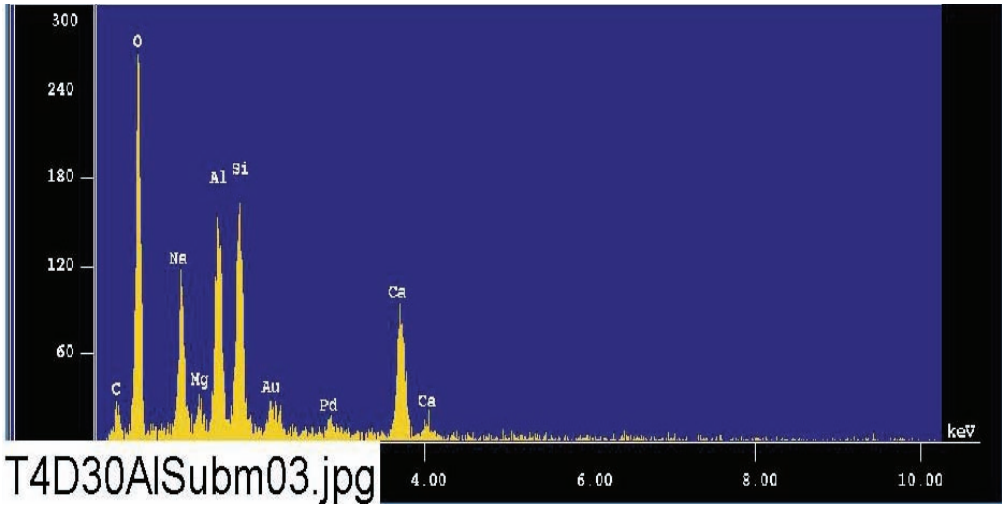

Figure 4-166. EDS counting spectrum for the deposits (EDS3) on the coupon surface shown in Figure 4-165. (T4D30AlSubm03.jpg)

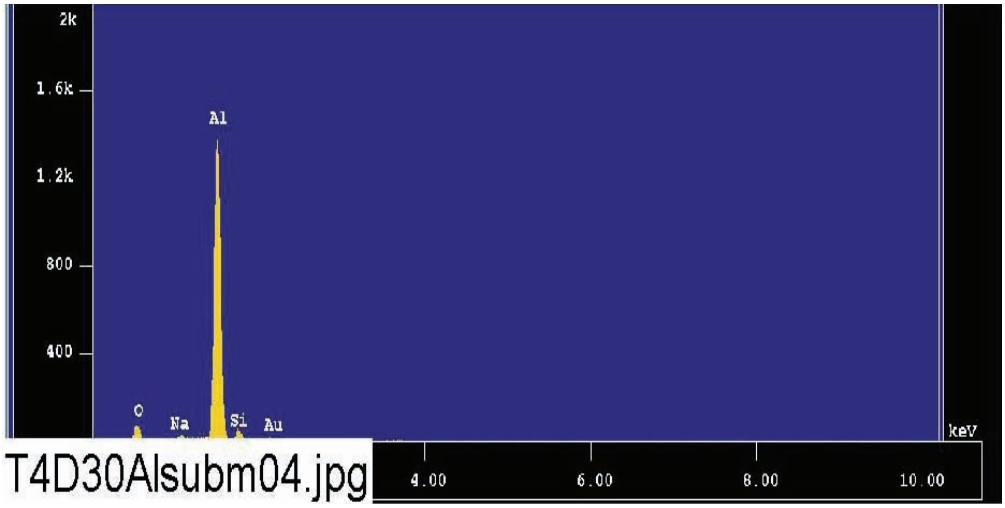

Figure 4-167. EDS counting spectrum for the flat coupon surface (EDS4), as shown in Figure 4-165. (T4D30AlSubm04.jpg)

Table 4-12. Elemental Compositions (by Mass %) of the Deposits and the Aluminum Coupon Surface, as Shown in Figure 4-163

Type	Al	Si	O	Ca	Na	Mg	C
Deposits (EDS3)	9.8	8.5	57.5	10.5	10.1	1.5	2.0
Submerged Aluminum Coupon Surface (EDS4)	74.6	3.5	20.7	N/D[a]	1.2	N/D	N/D

[a]N/D: Not detected

SEM images of an aluminum coupon after 30 days of submersion in Test #1 are shown in Figures 4-168 and 4-169. In contrast to Test #4, the SEM images show that the submerged aluminum coupon from Test #1 was rough and had many cracks, whereas the Test #4 aluminum coupon was smooth and integrated. EDS analyses associated with this coupon from Test #1 are shown in Figures 4-170 and 4-171. The elemental composition associated with this EDS analysis is presented in Table 4-13. From this analysis it is seen that silicon also was present on the aluminum coupon surface. Thus, it is possible that an insoluble aluminum silicate was responsible for passivating the aluminum coupons according to the following scenario. In Test #1, the aqueous silica concentration was low, and passivation did not occur until a high aluminum concentration was reached. In Test #4, passivation was achieved with a low aluminum concentration because the silica concentration was higher. A higher silica concentration in Test #4 solution was effective in forming a dense passivation layer on the submerged aluminum coupon surface. As a result, the corrosion was much less in Test #4. It should be noted that calcium might also have contributed to the passivation on the aluminum coupons. However, EDS results do not show the presence of calcium on the Test #4 aluminum coupon surface, except for loose deposits. Therefore, it is less likely that calcium was important for passivation in Test #4.

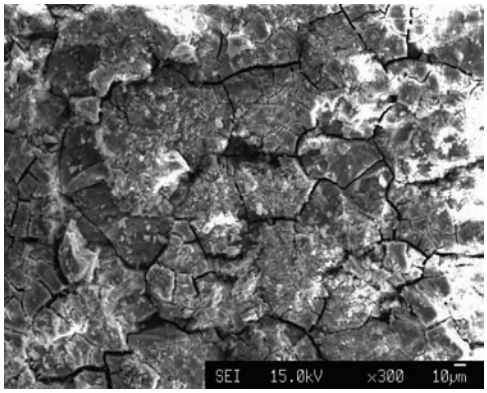

Figure 4-168. SEM image, magnified 300 times, of a Test #1, Day 30, submerged aluminum coupon sample. (Test1submAl015.bmp)

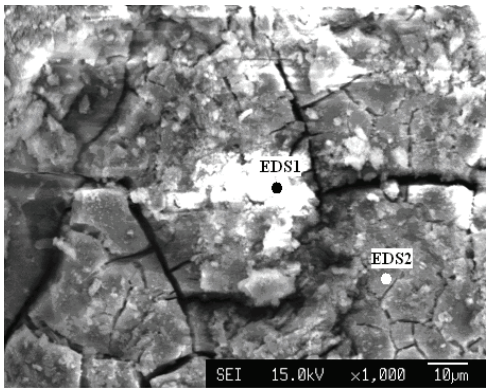

Figure 4-169. SEM image, magnified 1000 times, of a Test #1, Day 30, submerged aluminum coupon sample. (Test1submAl016.bmp)

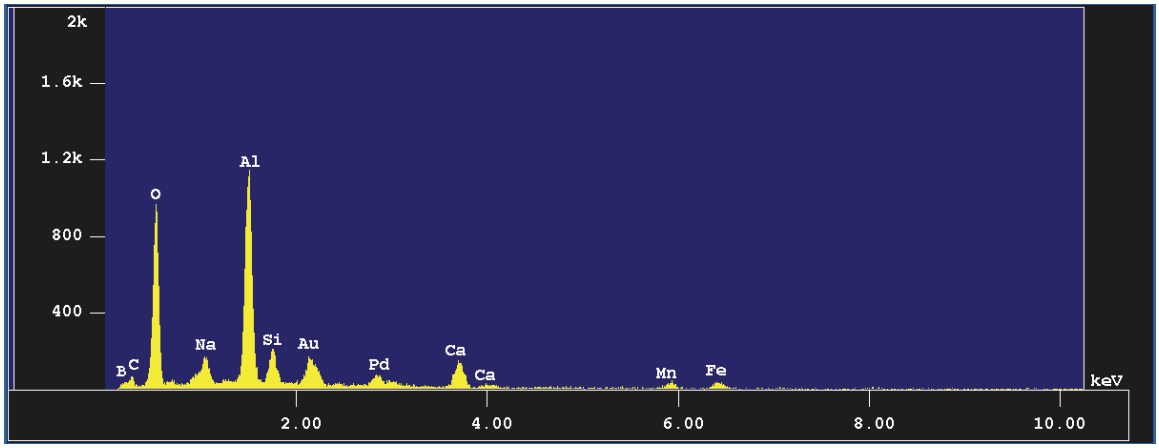

Figure 4-170. EDS counting spectrum for the light spot (EDS1) on the coupon surface shown in Figure 4-169. (T1AlEDS10.tif)

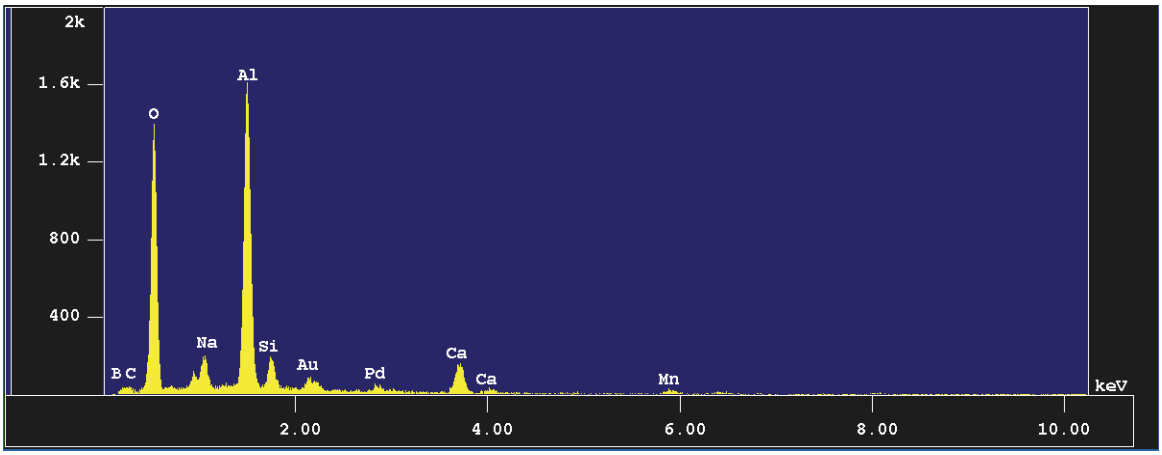

Figure 4-171. EDS counting spectrum for the grey coupon surface (EDS2) shown in Figure 4-169. (T1AlEDS11.tif)

Table 4-13. Elemental Compositions (by Mass %) of the Light and Grey Coating on the Aluminum Coupon Surface, as Shown in Figure 4-167

Type	Al	Si	O	Ca	Na	Mn	C	B	Fe
Light Coating (EDS1)	15.4	2.7	54.3	4.4	2.3	3.9	0	13.2	3.9
Grey Coating (EDS2)	18.4	2.2	60.8	4.6	2.4	2.7	0	8.9	N/D[a]

[a]N/D: Not detected

4.5. Deposition Products

Another phenomenon of interest in the ICET tests is the presence of deposition products because of corrosion, chemical precipitation, and/or physical sedimentation. These deposition products were fine powders that were extracted from horizontal and/or vertical pieces of the submerged CPVC coupon rack. Beginning with Test #2, deposition products were collected after each of the ICET tests was completed. The deposition products were collected by directly adhering the sample onto double-sided carbon tape suitable for SEM/EDS examination. After the samples were dried in air, a gold/palladium coating was applied to enhance the surface conductivity of the samples and to prevent possible charging problems during the SEM examination.

In general, the deposition products were composed of a variety of substances including insulation debris material (i.e., fiberglass and cal-sil), chemical precipitates, corrosion products, and other substances. In Tests #2 and #5, 100% of the insulation material was fiberglass; consequently, fiberglass debris was observed in the deposition products of these tests. In contrast, 80% of the fiberglass was replaced with cal-sil in Tests #3 and #4; as a result, cal-sil particles were likely present in the deposition products in these tests. In addition, because TSP was used in Tests #2 and #3, phosphorus was found in the elemental composition of the deposition products in those tests. This fact suggests that phosphate likely reacted with metal cations in the test solution and formed precipitates as deposition products. In addition, in Test #2, some white residues on a horizontal piece of the submerged CPVC rack were found to be rich in zinc. The result suggests that the residues likely originated from galvanized steel corrosion products.

Test #2 Deposition Products

Figures 4-172 and 4-173 show the SEM images of the deposition products collected from a vertical section of the submerged CPVC rack. In Figure 4-172, the cylindrical debris appears to be fiberglass, which mixed with other corrosion/precipitation products and debris. EDS results from Figure 4-174 indicate that the deposition products shown in Figure 4-173 were composed mainly of oxygen, phosphorus, magnesium, and carbon, with small amounts of aluminum, silicon, calcium, and sodium. Because TSP was used in Test #2, a precipitate of phosphate salts such as magnesium phosphate may have deposited on the submerged CPVC rack, in addition to other carbonate and metallic salts precipitates.

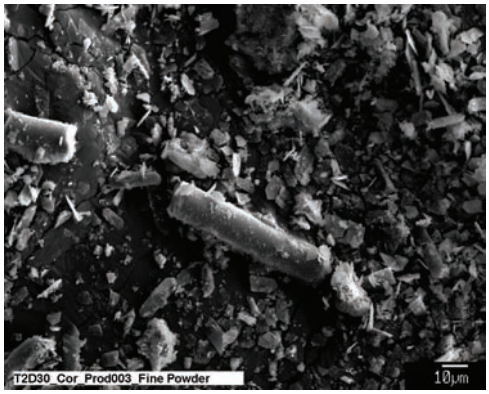

Figure 4-172. SEM image at 650× magnification of a Test #2, Day 30, sample of fine powder on a vertical piece of the submerged PVC rack. (T2D30_Cor_Prod003_Fine Powder)

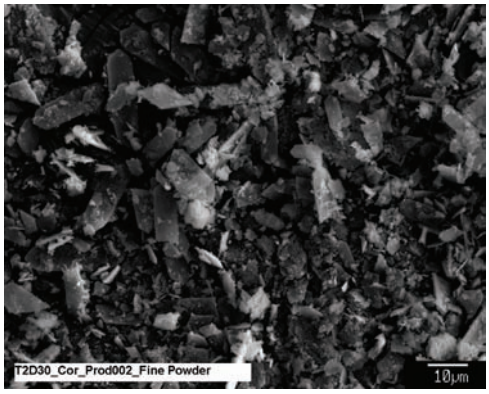

Figure 4-173. SEM image at 1000× magnification of a Test #2, Day 30, sample of fine powder on a vertical piece of the submerged PVC rack. (T2D30_Cor_Prod002_Fine Powder)

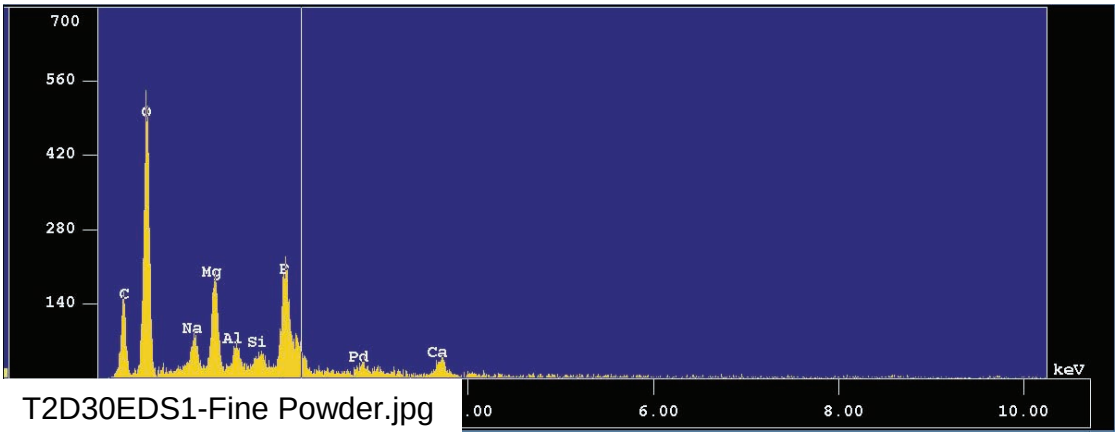

Figure 4-174. EDS counting spectrum for the entire SEM image shown in Figure 4-173. (T2D30EDS1-Fine Powder)

In addition, some white particulate residues were collected from a horizontal piece of the submerged CPVC rack and examined. The SEM image and EDS spectrum are shown in Figures 4-175 and 4-176, respectively. Semi-quantitative EDS results indicate that the mass composition of the white residue was primarily zinc, carbon, and oxygen, with smaller amounts of other

elements, as shown in Table 4-14. Because of a high zinc content in the substance, it is likely that the white residue originated from the corrosion products of galvanized steel, which peeled off the coupon and subsequently settled on the horizontal piece of the submerged CPVC rack.

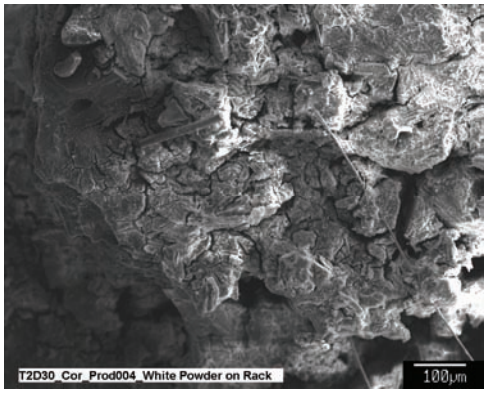

Figure 4-175. SEM image (130×) of a Test #2, Day 30, sample of white residue on a horizontal piece of the submerged CPVC rack. (T2D30_Cor_Prod004_White Powder on Rack)

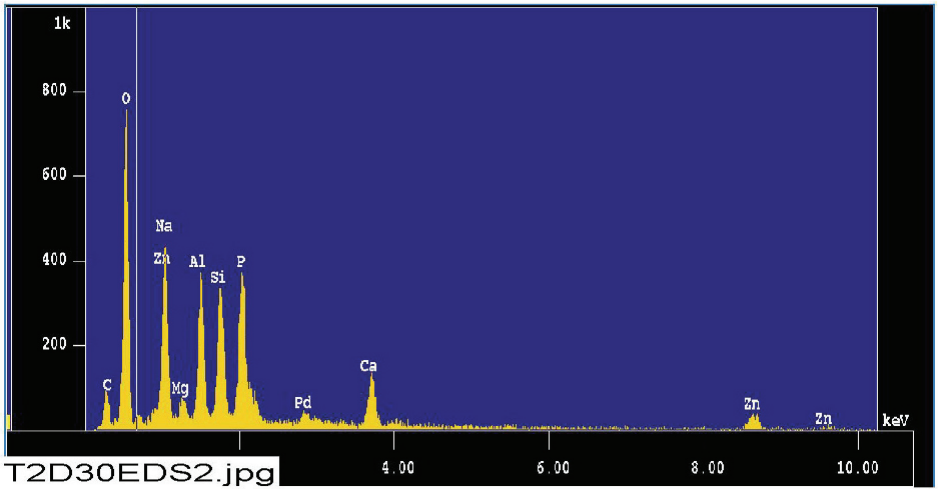

Figure 4-176. EDS counting spectrum for the white residue shown in Figure 4-175. (T2D30EDS2)

Table 4-14. Elemental Composition of Deposition Products Collected from Horizontal Surfaces on CPVC Coupon Racks after Tests Were Complete

Element	Test #2	Test #3	Test #4	Test #5
C	27	N/D[a]	1	35
O	39	48	52	50
Na	2	1	8	2
Mg	1	N/D[a]	N/D[a]	1
Al	4	N/D[a]	4	5
Si	4	3	15	6
P	6	13	N/D[a]	N/D[a]
Ca	3	34	19	2
Zn	14	N/D[a]	N/D[a]	N/D[a]
Likely dominant product	Zinc oxides, zinc carbonates	Calcium phosphate	Cal-sil	Carbonates

[a]N/D: Not detected.

Test #3 Deposition Products

After completion of Test #3, the fine powders on a horizontal piece of the submerged CPVC rack were collected for SEM/EDS analysis, and results are shown in Figures 4-177 and 4-178. Figure 4-177 indicates that the deposition products were composed mainly of particulate substances. The semi-quantitative EDS elemental analysis results show that the deposition products were composed mainly of calcium, phosphorus, and oxygen, with small amounts of sodium and silicon, as shown in Table 4-12. Because 80% of the fiberglass was replaced by cal-sil and TSP was used in Test #3, the deposition products are likely composed of precipitates such as calcium phosphate and cal-sil debris.

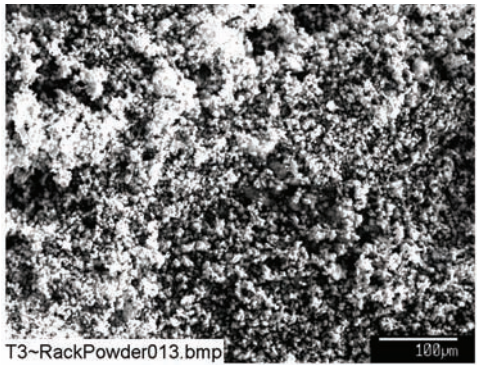

Figure 4-177. SEM image, magnified 200 times, of a Test #3, Day 30, powder on the submerged rack. (T3~RackPowder013)

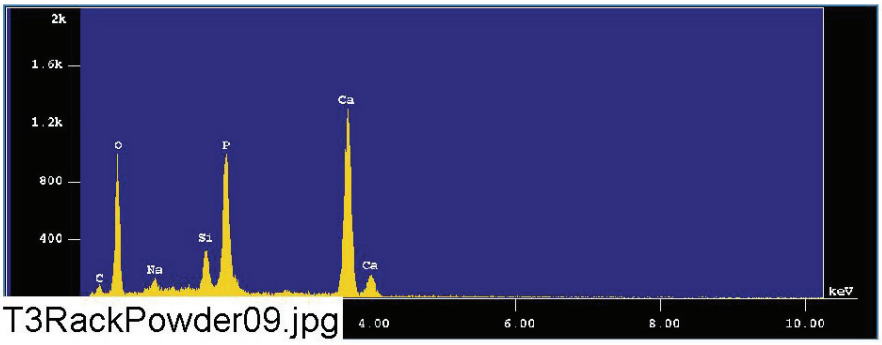

Figure 4-178. EDS counting spectrum for the powder on the submerged rack shown in Figure 4-177. (T3RackPowder09)

Test #4 Deposition Products

Fine powders on a horizontal piece of the submerged CPVC rack were collected when Test #4 ended. Figure 4-179 indicates that the deposition products were composed mainly of particulate substances. The EDS results are shown in Figure 4-180. Further semi-quantitative elemental analyses results indicated that the deposition products were composed mainly of calcium, silicon, oxygen, and small amounts of sodium, aluminum, and carbon, as shown in Table 4-14. Because 80% of the fiberglass was replaced by cal-sil and no TSP was used in Test #4, the deposition products likely are composed of cal-sil debris and other chemical precipitates.

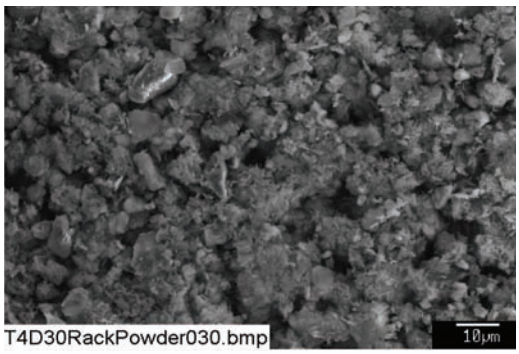

Figure 4-179. SEM image, magnified 1000 times, of a Test #4, Day 30, fine powder on the submerged rack. (T4D30RackPowder030.bmp)

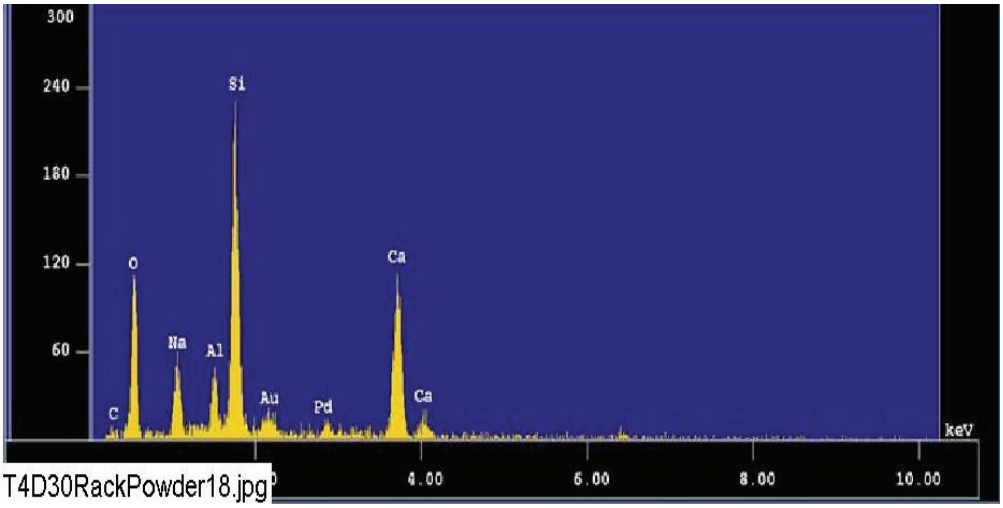

Figure 4-180. EDS counting spectrum for the particles (whole image) shown in Figure 4-179. (T4D30RackPowder18.jpg)

Test #5 Deposition Products

The deposition products collected upon completion of Test #5 were fine yellow powders that had deposited on a horizontal piece of the submerged CPVC rack. The SEM images of the deposition products are shown in Figures 4-181 and 4-182. From the figures, the deposition products were composed mainly of fiberglass debris and other substances. (Note that cal-sil was used only in Tests #3 and #4). The yellow color of the deposition products is consistent with the color of the fiberglass used in the test. Figure 4-183 shows the EDS spectrum of a particle as labeled in Figure 4-182, which was composed of carbon and oxygen, with smaller amounts of aluminum, silicon, sodium, calcium, and magnesium, as summarized in Table 4-14. As a result, the substance was likely a carbonate precipitate.

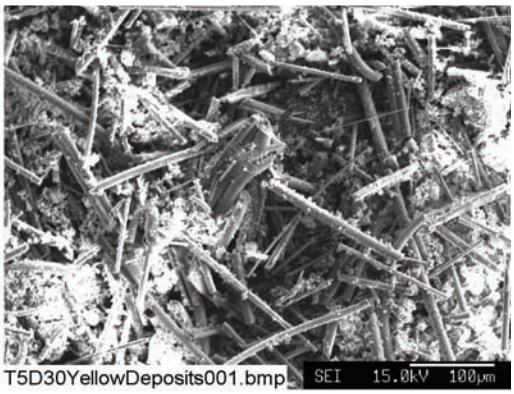

Figure 4-181. SEM image, magnified 100 times, of the Test #5 Day 30, fine yellow powder on the submerged rack. (T5D30YellowDeposits001.bmp)

Figure 4-182. Annotated SEM image, magnified 1000 times, for the Test #5, Day 30, fine yellow powder on the submerged rack. (T5D30YellowDeposits003.bmp)

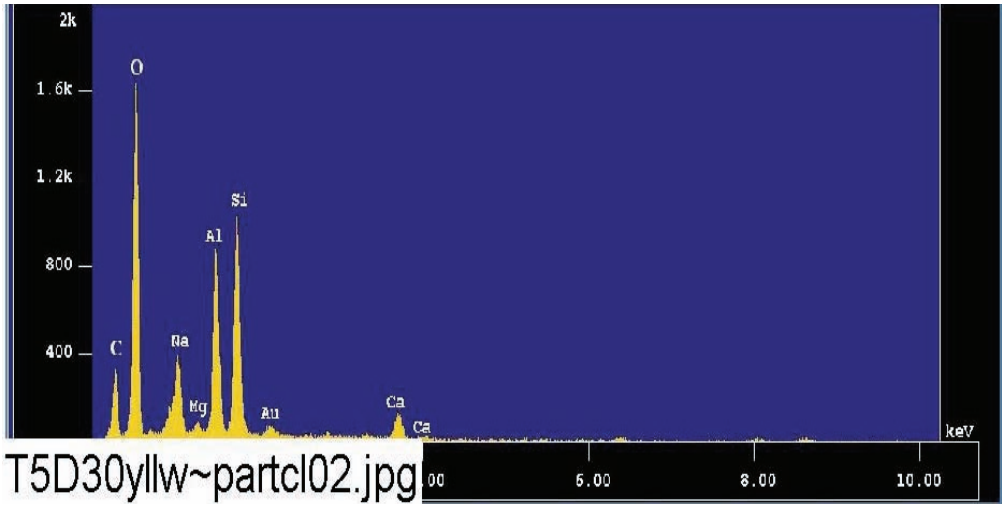

Figure 4-183. EDS counting spectrum for the particulate deposit shown in Figure 4-182. (T5D30yllw~partcl02.jpg)

4.6. Gel Analysis

There were two unique observations from ICET Test #3. First, a significant amount of white gel-like precipitates were observed in the test solution for several hours on the first day of the test during and after the injection of TSP. Looking through the tank's submerged view window, the test solution appeared to be nearly saturated with these precipitates that were moving robustly in a circular pattern. Second, when the test was completed, deposits of pinkish-white gel-like material were found on the top of the sediment and on other objects on the tank bottom. This material covered the majority of objects on the tank bottom including the birdcage, but it was not a continuous covering. Figures 4-184 and 4-185 are photographs of the gel-like material.

Figure 4-184. Stainless steel mesh covered with gel-like material.

Figure 4-185. Gel-like material recovered from the bottom of the tank.

SEM images of the gel-like material are shown in Figures 4-186 and 4-187. EDS results (Figure 4-188 and Table 4-15) indicated that 92% of the gel-like material was composed of calcium, oxygen, and phosphorus. Comparable ESEM and EDS images are shown in Figures 4-189 and 4-190. Consistently, XRF results (Table 4-16) indicated that the gel-like precipitates contained significant amounts of calcium and phosphorus. Therefore, it is likely that the gel-like material was $Ca_3(PO_4)_2$. In addition, EDS and XRF results indicated that the gel-like material had a small amount of carbon, possibly resulting from carbonate (CO_3^{2-}) and/or organic carbon from the test solution.

Based on water quality modeling using Visual Minteq 2.30 and on XRD results (Figure 4-191), the white gel-like material contained crystalline substances of $Ca_5(PO_4)_3OH$ (hydroxylapatite), $Ca_9HPO_4(PO_4)_5OH$ (calcium hydrogen phosphate hydroxide), and $Ca_3(PO_4)_2 \cdot xH_2O$ (calcium phosphate hydrate). It should be noted that XRD can detect only crystalline substances. Consequently, any amorphous substances would not be reflected in the XRD results.

Significant amounts of the gel-like material were deposited on top of the birdcage. SEM/EDS analyses were performed to compare the gel-like material on top of the birdcage with the particulate deposits on the exterior of fiberglass samples taken from inside the birdcage. Those analyses showed that their compositions were not exactly the same. The gel-like material contained higher amounts of phosphorus and lower amounts of silicon than did the particulate deposits on the fiberglass. As with any SEM sample, the gel-like material was dried before the analyses. Because its consistency was similar to that of a thick slurry, the drying process was unlikely to affect the major solid composition of the sample.

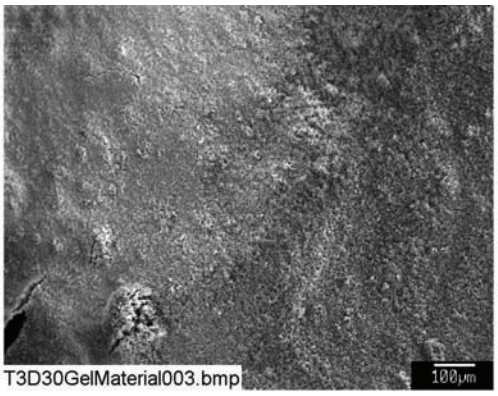

Figure 4-186. SEM image of a Test #3, Day 30, white gel-like material from the top of the birdcage, magnified 100 times. (T3D30GelMaterial003, 5/9/05)

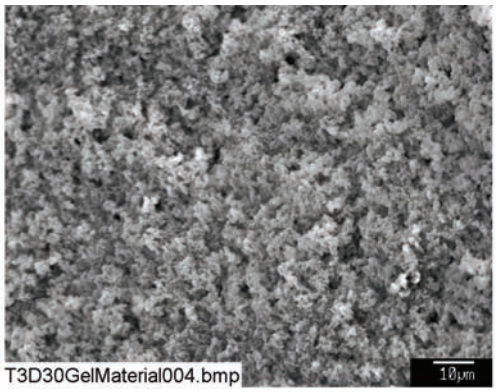

Figure 4-187. SEM image of a Test #3, Day 30, white gel-like material from the top of the birdcage, magnified 1000 times. (T3D30GelMaterial004, 5/9/05)

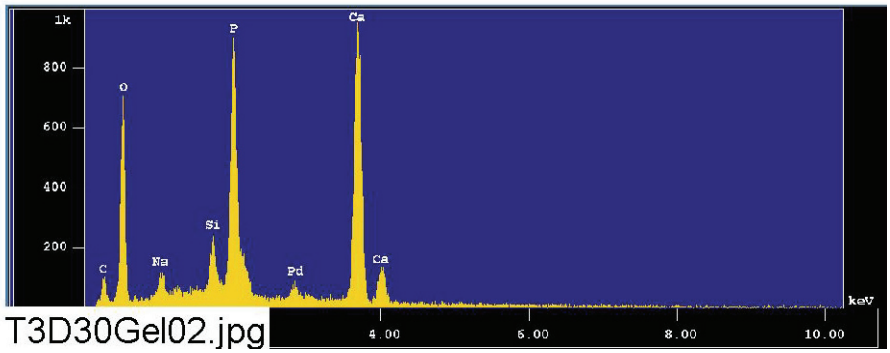

Figure 4-188. EDS counting spectrum for the white, gel-like material (whole image) shown in Figure 4-187. (T3D30Gel02, 5/9/05)

Table 4-15. The Chemical Compositions for Figure 4-188

May 9 2005

Group : NRC
Sample : T3D30 ID# : 2
Comment : GelMaterial
Condition : Full Scale : 20KeV(10eV/ch,2Kch)
Live Time : 60.000 sec Aperture # : 1
Acc. Volt : 15.0 KV Probe Current : 1.606E-09 A
Stage Point : X=79.625 Y=59.260 Z=11.424
Acq. Date : Mon May 9 11:42:11 2005

Element	Mode	ROI(KeV)	K-ratio(%)	+/-	Net/Background
C K	Normal	0.09- 0.46	0.6057	0.0005	338 / 119
O K	Normal	0.25- 0.77	12.2043	0.0032	4587 / 68
Na K	Normal	0.81- 1.27	0.5675	0.0010	613 / 50
Si K	Normal	1.50- 2.05	0.9391	0.0005	1366 / 271
P K	Normal	1.75- 2.38	8.4975	0.0055	7628 / 107
Ca K	Normal	3.39- 4.30	17.1295	0.0038	12109 / 26

Chi_square = 42.7915

Element	Mass%	Atomic%	ZAF	Z	A	F
C	4.355	7.8616	3.7318	1.0194	3.6611	0.9999
O	45.521	61.6928	1.9361	0.9721	1.9917	1.0000
Na	1.639	1.5456	1.4989	1.0256	1.4614	1.0000
Si	2.072	1.5994	1.1451	0.9756	1.1812	0.9937
P	13.776	9.6435	0.8415	1.1708	0.7203	0.9978
Ca	32.638	17.6571	0.9890	0.9947	0.9943	1.0000

Total 100.000 100.0000
Normalization factor = 1.9265
Total 100.000 100.0000
Normalization factor = 2.1120

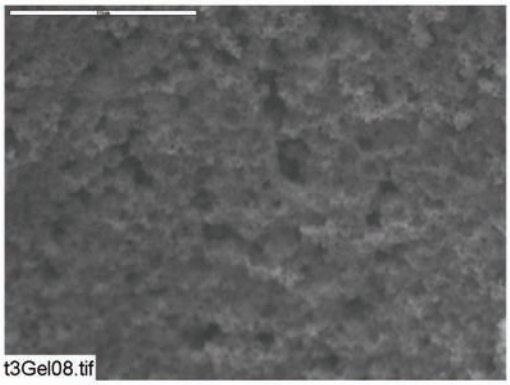

Figure 4-189. ESEM image of a Test #3, Day 30, white gel-like material from the top of the birdcage, magnified 1000 times. (t3Gel08, 5/6/05)

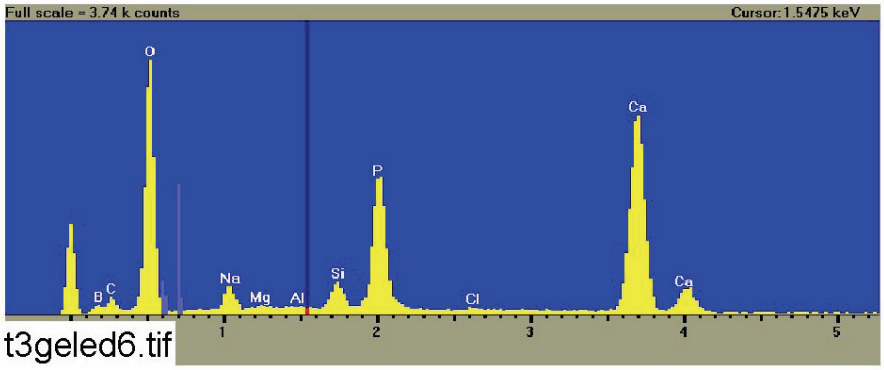

Figure 4-190. EDS counting spectrum for the white, gel-like material shown in Figure 4-189. (t3geled6, 5/6/05)

Table 4-16. Dry Mass Composition (%) of a Test #3 Day 30, White Gel-Like Sample by XRF Analysis

Compound	%
SiO_2	5.26
TiO_2	0.02
Al_2O_3	0.63
Fe_2O_3	0.07
FeO	0.00
MnO	0.00
MgO	0.25
CaO	35.01
Na_2O	2.39
K_2O	0.06
P_2O_5	27.09
$H_2O(-)$	4.75
$H_2O(+)CO_2$	19.24
Total	94.77

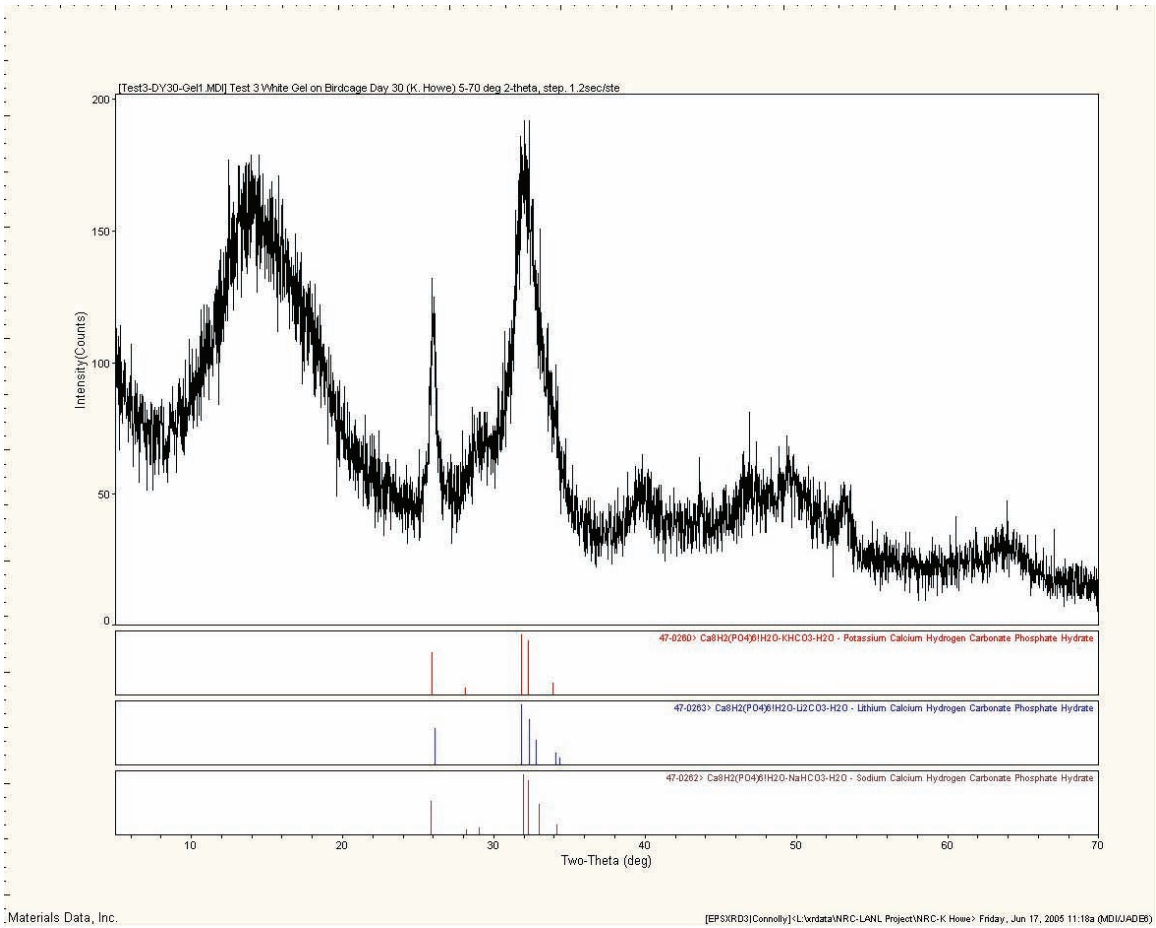

Figure 4-191. XRD results for a Test #3, Day 30, white gel-like sample.

This page intentionally left blank.

5. CONCLUSIONS

The primary objectives for the ICET test series were (1) to determine, characterize, and quantify chemical-reaction products that may develop in the containment sump under a representative post-LOCA environment and (2) to determine and quantify any gelatinous material that might be produced during the post-LOCA recirculation phase. Five tests were performed under different conditions, and they produced a variety of results.

In Test #1, the submerged aluminum coupons experienced a prominent reduction in mass over the 30 days of testing, which was attributable to the system pH of 9.4–9.5. Aluminum was detected in the test solution shortly after the test began and rose to a maximum pseudo-steady-state concentration of ~350 mg/L after 20 days. This increase in soluble aluminum is characteristic of continuous corrosion and subsequent passivation of the coupons, possibly caused by aluminum silicates, which occurred late in the test.

Although the presence of a gelatinous substance was not visually detected at the test temperature (60°C) during the entire test, chemical product precipitation occurred upon reduction of the solution temperature. The precipitate appeared to form more rapidly and in larger amounts over the test duration. ICP analysis of the precipitate revealed that it was composed largely of aluminum, sodium, and boron. TEM analysis helped determine that the precipitate was amorphous in nature. It was also noted that the precipitate did not fully re-dissolve when the solution was reheated.

Other observations were consistent with the presence of precipitates in the Test #1 solution. At 23°C, the turbidity was greater than at 60°C, and it increased over the duration of the test. Kinematic viscosity at 23°C was also greater than at 60°C, and it increased as the test progressed. The test solution was Newtonian at test temperature. However, at 25°C it demonstrated shear thinning, a characteristic of a non-Newtonian fluid.

Test #2 system interactions did not produce significant amounts of chemical precipitates or gelatinous material in the test solution. The system pH of 7 provided an environment of low corrosion of the metal coupons, which limited the effect of a complicated chemical environment. The observed chemical deposits, upon analysis of the fiberglass within the system, were attributed to the chemical byproducts formed in the test or from the drying process for sample analysis.

Analysis of the Test #3 system revealed large amounts of chemical precipitation and significant amounts of a gel-like material. Chemical precipitation occurred in solution at the test temperature during the first 4 hours of testing but was not observed afterwards, even on cooling, throughout the remainder of the test. During the test, the pH increased from 7.3 to 8, which decreased the buffering capability of the system and allowed for corrosion.

After the test solution was drained from the tank, a gel-like material was found as the top layer of the large sediment bed at the bottom of the tank, as well as on insulation samples placed within the tank. EDS results from the gel-like layer showed that 92% of the deposit was composed of calcium, oxygen, and phosphorus. It is likely that this layer was composed largely of $Ca_3(PO_4)_2$. Based on XRD results, the gel-like precipitates contained crystalline substances. Analysis of the

insulation samples showed large amounts of deposits on the exterior of the samples, which increased as the test progressed. The interior of the fiberglass was relatively pristine. Phosphorus was present on the outside surface of some of the submerged cal-sil chunks, while no significant phosphorus was found in the interior part of the cal-sil chunks. Analysis of the sediment suggested that it consisted largely of the cal-sil that was added at the beginning of the test, as well as fiberglass insulation and corrosion products.

During Test #4, large amounts of chemical deposit were detected on the fiberglass insulation samples as in Test #3. No measurable amount of chemical precipitates or gelatinous structures was detected in the test solution. A system pH of 9.8 was expected to promote the corrosion of the aluminum coupons; yet very little corrosion occurred. The lack of corrosion is hypothesized to result from passivation by an insoluble aluminum silicate coating on the coupons. This hypothesis is supported by EDS analysis of the coupons and solution chemistry.

The Test #5 environment did produce small amounts of chemical precipitates when the test solution cooled, but not at the test temperature. The precipitates took several days to form, and their quantity did not increase appreciably over the test duration. The presence of a gelatinous substance was not detected during the test. Aluminum was detected in the test solution shortly after the test began and rose to a maximum concentration of ~50 mg/L by the middle of the test. The presence of aluminum in solution was attributable to the system pH of 8.2 to 8.5, which promoted aluminum corrosion. When the solution cooled, small amounts of precipitate were observed. The precipitates were composed largely of aluminum, boron, calcium, and sodium. Few, if any, deposits were detected on the fiberglass samples obtained from the tank.

Behavior of the Test #5 test solution at 23°C was similar to the behavior of the Test #1 solution at the same temperature. Turbidity and kinematic viscosity at 23°C were greater than at 60°C, although they did not increase significantly throughout the test. The solution also exhibited shear thinning at 25°C, indicative of a non-Newtonian fluid.

The ICET series used three different buffering agents. When comparing these agents, sodium hydroxide and sodium tetraborate produced a solution pH that facilitated corrosion of the submerged aluminum coupons. Corrosion of the aluminum coupons could lead to the formation of chemical precipitates, which could transform to gelatinous products upon temperature reduction. The presence of cal-sil in the Test #4, high-pH system appeared to inhibit corrosion of the coupons, thus limiting the chemical constituents' formation of precipitates during decreases in temperature. Trisodium phosphate provided a neutral pH of 7, which had a decreased effect on the promotion of corrosion. When cal-sil was mixed into the Test #3 trisodium phosphate system, large amounts of chemical precipitation quickly occurred, and the formation of a gel-like material was observed.

The particle size distribution of the test solution was monitored throughout each of the five ICET tests. In Test #1, the particle size was smaller than 1 μm. In the other tests, the particle size distribution remained within the range of 1 to 100 μm. The distribution within that range varied from test to test.

6. REFERENCES

1. "Test Plan: Characterization of Chemical and Corrosion Effects Potentially Occurring inside a PWR Containment Following a LOCA, Rev. 13," July 20, 2005.

2. J. Dallman, J. Garcia, M. Klasky, B. Letellier, and K. Howe, "Integrated Chemical Effects Test Project: Test #1 Data Report," NUREG/CR-6914, Volume 2, U.S. Nuclear Regulatory Commission, Washington, D.C., 2006.

3. J. Dallman, B. Letellier, J. Garcia, M. Klasky, W. Roesch, J. Madrid, K. Howe, and D. Chen, "Integrated Chemical Effects Test Project: Test #2 Data Report," NUREG/CR-6914, Volume 3, U.S. Nuclear Regulatory Commission, Washington, D.C., 2006.

4. J. Dallman, B. Letellier, J. Garcia, J. Madrid, W. Roesch, D. Chen, K. Howe, L. Archuleta, and F. Sciacca, "Integrated Chemical Effects Test Project: Test #3 Data Report," NUREG/CR-6914, Volume 4, U.S. Nuclear Regulatory Commission, Washington, D.C., 2006.

5. J. Dallman, B. Letellier, J. Garcia, J. Madrid, W. Roesch, D. Chen, K. Howe, L. Archuleta, and F. Sciacca, "Integrated Chemical Effects Test Project: Test #4 Data Report," NUREG/CR-6914, Volume 5, U.S. Nuclear Regulatory Commission, Washington, D.C., 2006.

6. J. Dallman, B. Letellier, J. Garcia, J. Madrid, W. Roesch, D. Chen, K. Howe, L. Archuleta, and F. Sciacca, "Integrated Chemical Effects Test Project: Test #5 Data Report," NUREG/CR-6914, Volume 6, U.S. Nuclear Regulatory Commission, Washington, D.C., 2006.

7. K. Kasza, J. H. Park, B. Fisher, J. Oras, K. Natesan, and W. J. Shack, "Chemical Effects Head-Loss Research in Support of Generic Safety Issue 191," NUREG/CR-6913, U.S. Nuclear Regulatory Commission, Washington, D.C., 2006.

8. This reference is intentionally omitted.

9. *CRC Handbook of Chemistry and Physics*, 83rd edition, D. R. Lide, Ed. (CRC Press) 2002.

10. Corrosion of Aluminum and Aluminum Alloy, J. R. Davis, Ed. (ASM International: Materials Park, Ohio) p. 27, 1999.

11. K. R. Trethewey, and J. Chamberlain, *Corrosion for Students of Science and Engineering* (Longman Scientific & Technical: Hong Kong) 1988.

12. M. Klasky, J. Zhang, M. Ding, B. Letellier, D. Chen, and K. Howe, "Aluminum Chemistry in Prototypical Post-LOCA PWR Containment Environment," NUREG/CR-6915, U.S. Nuclear Regulatory Commission, Washington, D.C., 2006.